JGR Atmospheres

RESEARCH ARTICLE
10.1029/2021JD035114

Special Section:
Atmospheric PM2.5 in China: physics, chemistry, measurements, and modeling

Real-Time Characterization of Aerosol Compositions, Sources, and Aging Processes in Guangzhou During PRIDE-GBA 2018 Campaign

Wei Chen[1,2,3,4,5], Yuqing Ye[1], Weiwei Hu[1,2,4,5], Huaishan Zhou[1,2,3,4,5], Tianle Pan[1,2,3,4,5], Yingkun Wang[1,2,3,4,5], Wei Song[1,2,4,5], Qicong Song[6], Chenshuo Ye[6], Chaomin Wang[6], Baolin Wang[7], Shan Huang[6], Bin Yuan[6], Ming Zhu[1,2,3,4,5], Xiufeng Lian[1,2,4,5], Guohua Zhang[1,2,4,5], Xinhui Bi[1,2,4,5], Fan Jiang[6], Junwen Liu[6], Francesco Canonaco[8,9], Andre S. H. Prevot[8], Min Shao[6], and Xinming Wang[1,2,3,4,5]

[1]State Key Laboratory of Organic Geochemistry, Guangzhou Institute of Geochemistry, Chinese Academy of Sciences, Guangzhou, China, [2]CAS Center for Excellence in Deep Earth Science, Guangzhou, China, [3]Chinese Academy of Sciences University, Beijing, China, [4]Guangdong-Hong Kong-Macao, Joint Laboratory for Environmental Pollution and Control, Guangzhou Institute of Geochemistry, Chinese Academy of Science, Guangzhou, China, [5]Guangdong Provincial Key Laboratory of Environmental Protection and Resources Utilization, Chinese Academy of Science, Guangzhou, China, [6]Institute for Environmental and Climate Research, Jinan University, Guangzhou, China, [7]School of Environmental Science and Engineering, Qilu University of Technology (Shandong Academy of Sciences), Jinan, China, [8]Paul Scherrer Institute, Laboratory of Atmospheric Chemistry, Villigen, Switzerland, [9]Datalystica Ltd., Park innovAARE, Villigen, Switzerland

Key Points:

- The promotion effects among aerosol liquid water contents, aerosol acidity, sulfate and nitrate formation in the haze periods were found
- Freshly formed secondary organic aerosols (SV-OOA) contributed substantially to OA/ΔCO enhancement during aging processes
- Long heterogeneous lifetime of ambient OA (>2 weeks) was found based on an in situ field-deployed oxidation flow reactor

Supporting Information:

Supporting Information may be found in the online version of this article.

Correspondence to:

W. Hu,
weiweihu@gig.ac.cn

Citation:

Chen, W., Ye, Y., Hu, W., Zhou, H., Pan, T., Wang, Y., et al. (2021). Real-time characterization of aerosol compositions, sources, and aging processes in Guangzhou during PRIDE-GBA 2018 campaign. *Journal of Geophysical Research: Atmospheres*, *126*, e2021JD035114. https://doi.org/10.1029/2021JD035114

Received 24 APR 2021
Accepted 24 JUL 2021

Abstract To investigate the chemical compositions, sources, and aging processes of submicron particles (PM_1), a comprehensive field campaign was conducted in Guangzhou urban area of China during the autumn (October–November) of 2018. The average mass concentration of PM_1 was 35.6 ± 20.8 μg m^{-3}, which was mainly contributed by organic aerosols (OA, 42%), then followed by sulfate (25%) and inorganic nitrate (11%). The inorganic nitrate was found to be the main driving component (up to ~50%) to account for the fast increase of PM_1 during the polluted periods of Guangzhou autumn. The promotion effects of sulfate, aerosol liquid water content, and particles acidity on nitrate formation were systematically discussed. Source apportionment results showed 72% of OA in Guangzhou autumn was contributed by secondary OA (SOA), and 28% of primary OA (POA), including vehicle emission related hydrocarbon-like OA (HOA, 16%), nitrogen-containing OA (NOA, 3%) and cooking OA (COA, 8%). To explore the aging processes of OA, the dynamic variations of OA and its oxidation level as a function of ambient photochemical age are shown. Using an in situ field-deployed oxidation flow reactor, the heterogeneous reaction rate coefficients of ambient POA with OH radicals (k_{OH}) were estimated to be 4.0–5.4 × 10^{-13} cm^3 $molecules^{-1}$ s^{-1}, which is equivalent to a lifetime of POA >2 weeks. The long heterogeneous lifetime of POA supports gas phase oxidation was the major pathway for ambient OA aging. The OH uptake coefficient (γ_{OH}) was estimated to be 0.76–0.84, underlining that OH radicals can be taken up efficiently on ambient aerosols.

1. Introduction

Fine particles (or fine aerosols), which can lead to haze formation in mega cities, have substantially impacted on air quality (Molina & Molina, 2004; Pope et al., 2009), climate (IPCC, 2018), and human health (Dockery, 2009; Poschl, 2005), and are causing great concerns to public society. With strict air quality control policy being carried out in China in recent years, annual $PM_{2.5}$ mass concentrations have continuously decreased (Lu et al., 2020; J. Wang, Zhao, et al., 2017; Y. C. Wang, Huang, et al., 2017; Q. Zhang et al., 2019), for example, during the year of 2015–2020, the annual mass concentrations of $PM_{2.5}$ in most areas of the Pearl River Delta (PRD) region ranged from >10 to ~34 μg m^{-3} and had already met the China National Ambient Air Quality Standard (CNAAQS) at 35 μg m^{-3} (GB3095-2012) (Lin et al., 2018; Ma et al., 2019; Yan et al., 2020), however, are still much higher than the air-quality guideline (AQG, 10 μg m^{-3}) from the World Health Organization (WHO) (WHO, 2006). The daily high $PM_{2.5}$ mass concentrations (up to ~100 μg m^{-3}) in the PRD region usually occurred in autumn to winter time, when the large anthropogenic emissions, complex chemical transformation and adverse meteorological condition happened (Chan & Yao, 2008; Fang

et al., 2019; Hou et al., 2019; Y. J. Li et al., 2017). While exclusive studies focus on the severe air pollution in the northern part of China (W. Hu, Hu, Hu, Jimenez, et al., 2016; W. Hu, Hu, et al., 2017; Huang et al., 2010; Zhao et al., 2013, and references therein), the aerosol formation mechanism in southern China, especially in the PRD region with a different aerosol source composition compared to the north due to the distinguished heating strategies and meteorology conditions, are still limited (W. Li, Liu, et al., 2018; Lu et al., 2019; Yue et al., 2010; Zhou et al., 2018). A thorough understanding of the formation mechanism of autumn to winter haze in the PRD region is of great significance on air pollution control and policy-making.

To achieve this purpose, the detection of dynamic variation of fine particle mass concentrations and chemical components at a high time resolution is necessary considering the wide emission sources and persistent physical meteorology impacts (Hallquist et al., 2009; Poschl, 2005; Seinfeld & Pandis, 2006). On-line aerosol mass spectrometer (AMS), a world-widely used instrument, is one of the most state-of-art techniques for quantifying the mass concentrations and size distributions of main components of aerosols at high time resolutions of seconds to minutes (Canagaratna et al., 2007; Jayne et al., 2000). By combining the organic aerosol (OA) spectral matrix with the source apportionment tool of positive matrix factorization (PMF) (Paatero & Tapper, 1994; Ulbrich et al., 2009) and/or the multi-linear engine (ME-2) (Canonaco et al., 2013; Paatero, 1999), the sources and evolution of OA in ambient air at a high time resolution can be identified and characterized. In addition, the oxidation levels of bulk OA (oxygen to carbon ratio, O:C; hydrogen to carbon ratio, H:C), which can provide crucial information for better understanding of SOA evolution and model simulation, can also be obtained (Aiken et al., 2008; Q. Chen et al., 2015; Jimenez et al., 2009).

Heterogeneous reactions can play pivotal roles for OA aging in the atmosphere (George & Abbatt, 2010; Kroll et al., 2015). Heterogeneous reactions of OA with OH radicals, characterized by reaction rate coefficients (k_{OH}), or alternatively, effective uptake coefficients of OH (γ_{OH}), defined as the fraction of OH radicals colliding with a compound that results in reactions, were usually explored in laboratory studies (Kessler et al., 2010; Slade & Knopf, 2014; Smith et al., 2009; Weitkamp et al., 2008). The k_{OH} and γ_{OH} can span a wide range of 0.25–34 $\times$ 10^{-12} cm^3 $molec^{-1}$ s^{-1} and <0.01 to >1, depending on the chemical compositions, phase state, mixing state and OH concentrations (Kessler et al., 2010, 2012; McNeill et al., 2008; Slade & Knopf, 2014; Weitkamp et al., 2008). The ambient OA, composed of several thousands of individual OA species, are usually much more complex than the laboratory-generated OA (Aiken et al., 2008; Burkholder et al., 2017). Investigating heterogeneous reaction processes with real ambient OA would be essential to understand the OA aging processes under ambient environment. The recent development of field-deployed oxidation flow reactor (OFR) has provided a unique opportunity to achieve this (Kang et al., 2007; Lambe et al., 2011; Ortega et al., 2016). By generating the OH radicals with UV-lamps in the OFR, the heterogeneous reaction rate of ambient aerosols with controlled OH radicals can be studied (W. Hu, Hu, Hu, Niu, et al., 2016).

To investigate the sources, chemical composition, and aging processes of fine particles in southern China, a comprehensive campaign was conducted during the autumn (October–November) in Guangzhou, which is a representative city in the PRD region. Previously, Cai et al. (2017) reported the diurnal variation and size distributions of main species in Guangzhou measured by an AMS and suggested ambient aerosols were mainly affected by traffic-related sources and industrial emissions. However, there was a lack of direct evidences from source apportionment results. J. Guo et al. (2020) investigated the sources of OA with an Aerosol Chemical Speciation Monitor (ACSM, simplified version of AMS), and suggested SOA formation during the polluted periods in Guangzhou was mainly governed by heterogeneous/multiphase reactions, while needs more accurate and direct evidences.

In this study, the chemical compositions and size distributions of submicron particles (PM_1) in autumn-winter of Guangzhou were quantified with an on-line AMS and other multiple start-of-art techniques. The formation mechanism of nitrate which was shown to be the main contributor for PM_1 enhancement during the polluted periods, was systematically discussed. The sources, elemental ratios, and evolution of ambient OA as a function of photochemical age were explored and compared with other literature results. Finally, the heterogeneous processes of ambient OA with OH radicals were studied in situ by taking advantages of a field-deployed OFR. To our knowledge, this is the first time that the γ_{OH} of ambient OA was estimated based on ambient aerosols in the urban areas.

2. Experimental Methods

2.1. Sampling Site Description

The campaign was carried out from October 1 to November 20, 2018 in the downtown of Guangzhou. The observation site (23.14°N, 113.36°E) was located at the top of a ninth floor building on the campus of Guangzhou Institute of Geochemistry (GIG), Chinese academy of sciences (CAS). The observation site was mainly surrounded by urban transportation, commercial and residential districts (Figures S1a–S2b) (C. Wang, Yuan, et al., 2020; Wu et al., 2020). The average ambient temperature and relative humidity (RH) in this campaign were 23.7 ± 2.9°C and 71.9 ± 17.4%, respectively. The site was mostly affected by northeasterly winds with an average speed of 4.5 ± 2.2 m s^{-1} (Table S1; Figure S1b).

2.2. HR-ToF-AMS Operation and Data Analysis

A High-Resolution Time-of-Flight AMS (HR-ToF-AMS, Aerodyne Research Inc. US; hereafter referred to as "AMS") was used to measure the mass concentrations and size distributions of main components in non-refractory PM_1 at a time resolution of 4 min. A $PM_{2.5}$ cyclone at 5 L min^{-1} was set in the upstream of sampling line to avoid blocking the AMS orifices from aerosols at large sizes. The sampling line made of stainless tubing was ~3 m long and a total residence time of 3 s was achieved. Two Nafion dryers were placed in the upstream of AMS sampling line to keep the RH of sampled air below 40% to eliminate the collection efficiency (CE) variation caused by particle phase state and morphology change due to high RH (Figure S1c) (Matthew et al., 2008).

The flow rates and particle size distributions were calibrated before and after the campaign. Ionization efficiency (IE) calibration using Brute-Force Single Particle (BFSP) method was conducted every 3–5 days using size-selected (400 nm) monodisperse pure ammonium nitrate (AN) particles. The variation of air beam versus IE in this study was within 4% (Figure S2a), suggesting a stable status of AMS during the entire campaign. Relative ionization efficiencies (RIEs) for ammonium (3.92), sulfate (1.22), and chloride (1.47) were calculated based on sampling their neutral salts in AMS, that is, NH_4NO_3, $(NH_4)_2SO_4$, and NH_4Cl (Figure S3). The default values of RIEs were used for OA (1.4) and nitrate (1.1) (Jimenez et al., 2016; Xu et al., 2018).

A chemical composition-based CE (CDCE) with an average value of 0.5 was estimated based on Middlebrook et al. (2012) (Figure S2c). The detection limit of each species in AMS HR mode is 0.172 (OA), 0.004 (NH_4), 0.011 (NO_3), 0.037 (SO_4), 0.008 (Cl) μg m^{-3}, respectively. Pieber et al. (2016) showed that artificial CO_2^+ signals can be detected and falsely recognized as OA signal in AMS due to the catalytical reactions between inorganic salts and organic residues on vaporizer surfaces. The CO_2^+/NO_3 ratio based on sampling pure NH_4NO_3 into AMS system is around 2.32% (Figure S4). The artificial CO_2^+ was subtracted based on this ratio when OA mass concentration and following data analysis including PMF and elemental ratios were obtained. In this campaign, the mass concentration of organic and inorganic nitrates were investigated using the NO_2^+/NO^+ method following Farmer et al. (2010) and Fry et al. (2013). The detailed description of the estimation process can be found in Section S3.

AMS V mode data were analyzed using Igor Pro 6.3.7 (WaveMetrics, Lake Oswego, OR) combining with the SQUIRREL 1.62C and PIKA 1.22C software. The elemental ratios of OA, including O:C, H:C, and OA to organic carbon ratio (OA:OC), were calculated based on the recalibrated "Improved-Ambient" method (Canagaratna et al., 2015). For comparison, elemental ratios reported in the previous studies based on Aiken et al. (2008) were multiplied by a ratio of 1.28 for O:C and 1.11 for H:C. The dynamic OA density was estimated using an empirical equation in Kuwata et al. (2011) based on IA corrected elemental ratios. Previous results showed the updated elemental ratio values from IA method are still valid for empirical OA density calculation equation (W. Hu, Campuzano-Jost, et al., 2017; W. Hu et al., 2020).

Unconstrained PMF and ME-2 engine were both applied to resolve the sources of OA based on the time-dependent OA high-resolution mass spectral matrix (V-mode, m/z 12–120). HR-MS data and error matrix were preprocessed for PMF analysis, including removing isotopes and "bad" ions (S/N ratio < 0.2), downweighing the "weak" ions (0.2 < S/N < 2) and m/z 44 related ions (Ulbrich et al., 2009). The final solution of five PMF factors was determined based on the characteristics of mass spectrum, time series, diurnal variation

patterns of resolved-factors, as well as their correlation with external tracers (Ulbrich et al., 2009; Q. Zhang et al., 2011). The detailed information on determination of PMF solutions with ambient data set can be found in Section S1.

2.3. Oxidation Flow Reactor (OFR)

Field-deployed OFR (Aerodyne Research Inc., US) has been developed recently to study in situ OA oxidation processes under ambient conditions (Kang et al., 2007; Lambe et al., 2011; Ortega et al., 2016; Sengupta et al., 2020). High concentration of OH radicals (10^8–10^{12} molecule cm^{-3}) can be formed in the OFR though initializing the photochemistry of O_3 and H_2O under UV light (R. Li, Palm, et al., 2015; Peng et al., 2015). The total flow rates through the OFR were in the range of 4.7–7.5 L min^{-1} corresponding to a calculated mean residence time of ~110–170 s for plug flow. The OH equivalent aging days in this study were varied from several hours to 14 days by assuming an average ambient OH concentration of 1.5×10^6 molecules cm^{-3} (Mao et al., 2009). This OH concentration of 1.5×10^6 molecules cm^{-3} is applied here for a better comparison with a wide range of previous studies in which the OH equivalent photochemical age was estimated using the same OH concentration (Hayes et al., 2013; W. Hu, Palm, et al., 2016; Nault et al., 2018; Ortega et al., 2016). This OH concentration of 1.5×10^6 molecules cm^{-3} is also similar to the ambient average OH concentration of 1.3×10^6 molecule cm^{-3} for this campaign, which was estimated based on a box model with MCM as mechanism (Z. Wang, Yuan, et al., 2020). During the campaign, VOCs and ambient aerosols were sampled and oxidized in the OFR for most of the time (October 20–November 21). To investigate the pure heterogeneous reaction of ambient OA, the ambient VOCs and other trace gas-phase species (e.g., NO_2, SO_2) were scrubbed by a denuder filled with activated carbons for a few days (December 6–Decemebr 12) to exclude the influences of gas-phase reaction on aerosol oxidation. The schematic setup of OFR setup can be found in Figure S1c.

2.4. Other Instrumentation

The ambient mass concentration of black carbon (BC) was measured by two aethalometers (AE31 for period October 1 to October 30 and AE-33 for period October 31 to November 20, Magee, U.S.) under the wavelength of 880 nm at a time resolution of 5 min (Drinovec et al., 2015). The ambient particle number size distribution (mobility diameter: 14.4–685.4 nm) was detected by a scanning mobility particle sizer (SMPS, TSI Inc.) at a time resolution of 4 min. Total mass concentration of PM_1 can be estimated based on multiplying the volume concentration obtained by SMPS with the dynamic aerosol density calculated from aerosol chemical composition measured by AMS and aethalometers (DeCarlo et al., 2008; W. Hu, Campuzano-Jost, et al., 2017). The average aerosol density during this campaign was 1.6 ± 0.1 g cm^{-3} (mean ± standard deviation). Online $PM_{2.5}$ mass concentration at a time resolution of half an hour was also monitored by BAM-1020 instrument (METONE, USA).

A commercial proton transfer reaction time-of-flight mass spectrometer (PTR-ToF-MS, Ionicon Analytic GmbH, Innsbruck, Austria) and an on-line GC-MS were used to measure various volatile organic compounds (VOCs) (C. Wang, Yuan, et al., 2020; Wu et al., 2020). A chemical ionization mass spectrometer coupled with FIGAERO inlet (FIGAERO-CIMS) was also applied for measuring the gas-phase N_2O_5 and cooking aerosol tracers, including oleic acid ($C_{18}H_{34}O_2$), linoleic acid ($C_{18}H_{32}O_2$), stearic acid ($C_{18}H_{36}O_2$), palmitic ($C_{16}H_{32}O_2$) and azelaic acid ($C_9H_{16}O_4$) (Ye et al., 2020). The concentrations of gas phase NO_2/NO, O_3 and CO were measured using the NO-NO_2-NO_x analyzer (42i, Thermo Fisher Scientific Inc., US), O_3 analyzer (49i, Thermo Fisher Scientific Inc., US) and CO analyzer (48i, Thermo Fisher Scientific Inc., US) at a time resolution of 1 min, respectively. The gas-phase NH_3 was measured by LGR-NH_3 analyzers (Model 902-0016, Los Gatos Research, USA).

3. Results and Discussion

3.1. Characterization of PM_1 Main Chemical Composition

The time series of PM_1 mass concentrations measured by AMS and Aethalometers (BC) showed good agreement with the integrated total aerosol mass concentrations from SMPS (slope = 1.06, R = 0.94), as well as

with $PM_{2.5}$ mass concentrations from an online instrument (slope = 1.02, R = 0.92) (Figure S5), validating the accuracy of AMS data measured in this study. Generally, the PM_1 mass concentrations showed large variation during the entire campaign, which ranged from 2.8 to 170.6 μg m^{-3} with an average value of 35.6 ± 20.8 μg m^{-3} (Table 1). Species of OA (including organic nitrate) and sulfate, accounting for 42% and 25% of the total PM_1 mass respectively, were the two most abundant components, then followed by inorganic nitrate (11%), ammonium (11%), black carbon (8%), and chloride (1%) (Figure 1h).

We categorized the time series of PM_1 to be two typical periods based on total PM_1 mass concentrations and meteorology conditions: (i) clean and (ii) polluted periods, as the background tint colors demonstrated in Figure 1. The clean periods (C1-C4) were mainly affected by clean air from the northern China at high wind speed of 6.6 m s^{-1} on average. The average mass concentration of PM_1 during the clean periods was ~ 20.9 ± 2.6 μg m^{-3}, dominated by OA and sulfate probably from long-range transport. BC was found to be mainly contributed by traffic emissions (85%, Figure S9) based on aethalometer measurement (Section S2) (Zotter et al., 2017). The high BC fraction (15%) during the clean periods was consistent with its local traffic emission origins. In this campaign, the polluted and clean periods usually alternated. Three polluted periods (P1–P3) were selected as shown in Figure 1, in which the mass loadings of ambient PM_1 (77.1 ± 22.1 μg m^{-3} in average) and other pollutants were greatly enhanced compared to those in the clean periods (Table 1). During the polluted periods, the static wind speed (<2 m s^{-1}) and high-pressure favored the accumulation of pollutants.

3.2. Inorganic Nitrate Formation and Its Driving Factors

Based on the source apportionment, >90% of total nitrate was inorganic nitrate during the polluted periods when nitrate concentration was >10 μg m^{-3} (Figure S10b). Inorganic nitrate was found to be the main driving component for the rapid increase of PM_1 during the polluted periods. The inorganic nitrate increased from ~10% to 30% as PM_1 mass concentrations got higher (several μg m^{-3} to above 100 μg m^{-3}) (Figure 1k). During the real-time pollution episodes (e.g., P2, P3), the increase rates of inorganic nitrate were around 0.71–0.79 μg m^{-3} h^{-1}, which can contribute up to 50% percent of PM_1 enhancement when balanced NH_4 masses were included, highlighting the substantial contributions of ammonium nitrate to the heavy pollution events. The increased domination of inorganic nitrate in fine particles during the highly polluted periods was consistently found in the other sites of PRD regions (Figure 2) (Gong et al., 2012; Griffith et al., 2015; He et al., 2011; Qin et al., 2017), as well as in the other vast areas of China, such as North China Plain (NCP) (W. Hu, Hu, Hu, Jimenez, et al., 2016; W. W. Hu et al., 2013; Huang et al., 2010; H. Li, Zhang, et al., 2018; Luo et al., 2020; Xu et al., 2019) and Yangtze River Delta (YRD) regions (H. Chen et al., 2020; Lin et al., 2020; W. Wang, Yu, et al., 2018; Y. Wang, Wang, et al., 2018). The fast formation of inorganic nitrate usually happened during the periods with strong photochemical chemistry facilitating the gas oxidation of NO_2 to HNO_3, and then forming semi-volatile NH_4NO_3 species or during high RH periods when the contribution of aqueous hydrolysis of N_2O_5 is substantial, especially during the nighttime (Y. L. Wang et al., 2019).

In this study, the inorganic nitrate formation was promoted during the polluted periods due to (a) the high concentrations of nitrate precursors. For example, the concentrations of nitrate precursors such as NO_2 (48.1 ppb in the polluted periods vs. 19.1 ppb in the clean periods) and N_2O_5 (319.2 vs. 91 ppt) were substantially elevated during the polluted periods. In addition, the formation of these gas precursors was also favorable due to increased oxidants of O_3 (from 12.9 to 25.0 ppb) from fast ROx cycling and higher oxidant precursor concentrations during the polluted periods (Table 1) (Fu et al., 2020).

(b) The favored inorganic nitrate formation pathways. In this part, the impacts of NH_3, RH, sulfate, aerosol liquid water contents (ALWC) and aerosol acidity (pH) on nitrate formation will be systematically discussed in the following. Based on the molar ratio of $[NH_4]/[SO_4] > 1.5$, the ammonium-rich conditions prevailed in the entire campaign (Figure S12a), suggesting there were excess NH_3 in the ambient air to react with HNO_3 to produce gas-phase NH_4NO_3 (Griffith et al., 2015; X. Liu et al., 2015). According to the deliquescence relative humidity (DRH) calculation for NH_4NO_3 in condensed phase (62.5% ± 1.5% by ln (DRH) = 723.7/T + 1.6954) (Seinfeld & Pandis, 2006), NH_4NO_3 during the polluted periods in this study mainly existed in the aqueous phase due to the higher ambient RH (~82.5 ± 5.5%). Under the saturated NH_3 and aqueous state conditions, the elevated sulfate mass concentrations during the polluted periods

Table 1
Average Mass Concentrations and Standard Deviation (SD) of Total PM_1 and Its Chemical Components, OA Factors, Gas Pollutants, and Metrological Parameters During the Entire Campaign, Clean Periods, and Polluted Periods

	Average ± SD		
	Average	Clean periods	Polluted periods
Total PM_1 ($\mu g\ m^{-3}$)	35.6 ± 20.8	20.9 ± 2.6	77.1 ± 22.1
Total PM_1 from SMPS ($\mu g\ m^{-3}$)	35.1 ± 18.6	17.1 ± 5.0	64.4 ± 14.1
$PM_{2.5}$ ($\mu g\ m^{-3}$)	36.5 ± 17.8	30.2 ± 3.9	60.2 ± 18.5
Total OA ($\mu g\ m^{-3}$)	14.7 ± 8.8	7.0 ± 1.5	28.6 ± 6.4
SV-OOA	3.8 ± 3.9	0.9 ± 0.7	8.0 ± 3.1
LV-OOA	5.9 ± 3.2	3.6 ± 1.2	5.7 ± 1.5
COA	2.2 ± 2.5	0.5 ± 0.6	5.0 ± 2.5
HOA	2.6 ± 3.0	1.2 ± 0.9	7.1 ± 3.5
NOA	0.5 ± 1.4	0.5 ± 0.2	0.7 ± 0.6
O:C	0.6 ± 0.1	0.8 ± 0.1	0.6 ± 0.1
H:C	1.6 ± 0.1	1.5 ± 0.1	1.6 ± 0.1
OA:OC	2.0 ± 0.2	2.1 ± 0.1	1.9 ± 0.1
Sulfate ($\mu g\ m^{-3}$)	8.9 ± 4.2	7.0 ± 1.2	13.4 ± 3.2
Total nitrate ($\mu g\ m^{-3}$)	4.5 ± 5.7	1.4 ± 0.7	14.8 ± 9.6
Inorganic nitrate ($\mu g\ m^{-3}$)	4.0 ± 5.7	1.3 ± 1.0	14.6 ± 9.7
Organic nitrate ($\mu g\ m^{-3}$)	0.6 ± 0.5	0.5 ± 0.2	0.3 ± 0.2
Ammonium ($\mu g\ m^{-3}$)	4.1 ± 2.7	2.6 ± 0.4	8.4 ± 3.7
Chloride ($\mu g\ m^{-3}$)	0.5 ± 0.7	0.16 ± 0.2	1.3 ± 0.9
BC ($\mu g\ m^{-3}$)	3.0 ± 1.4	2.7 ± 0.5	5.2 ± 1.2
Temperature (°C)	23.7 ± 3.9	21.2 ± 1.5	25.1 ± 1.6
RH (%)	71.9 ± 17.4	60.2 ± 5.6	82.5 ± 5.5
Wind speed ($m\ s^{-1}$)	4.5 ± 2.3	6.6 ± 1.5	1.5 ± 1.0
CO (ppm)	0.4 ± 0.1	0.5 ± 0.1	0.6 ± 0.1
NO (ppb)	12.1 ± 22.0	8.1 ± 9.0	32.4 ± 38.2
NO_2 (ppb)	32.1 ± 17.9	19.4 ± 5.8	48.1 ± 12.1
N_2O_5 (ppt)	66.4 ± 337.1	91.3 ± 162.7	319.2 ± 971.6
SO_2 (ppb)	1.9 ± 1.5	0.5 ± 0.3	2.2 ± 0.8
O_3 (ppb)	32.0 ± 30.5	12.9 ± 10.2	25.0 ± 32.2
NH_3 (ppb)	9.6 ± 3.5	7.7 ± 2.1	9.4 ± 2.0
ALWC ($\mu g\ m^{-3}$)	34.1 ± 41.6	7.0 ± 2.2	78.6 ± 55.4
pH	2.6 ± 0.6	1.6 ± 0.3	3.1 ± 0.3

ALWC, aerosol liquid water content; COA, cooking organic aerosol; HOA, hydrocarbon-like organic aerosol; NOA, nitrogen-containing OA; SMPS, scanning mobility particle sizer.

($13.4\ \mu g\ m^{-3}$ in the polluted periods vs. $7.0\ \mu g\ m^{-3}$ in the clean periods) would promote the inorganic nitrate formation in condensed phase not only by directly lowering the ion strength fraction of NH_4NO_3, thus decreasing equilibrium dissociation constant for favoring the partitioning of gas-phase NH_4NO_3 (Seinfeld & Pandis, 2006), but also through modulating ALWC and pH in an indirect way.

We further investigated the interaction of ALWC and pH with inorganic nitrate formation during the polluted periods. The ALWC and particle pH were estimated using the ISORROPIA-II thermodynamic model at forward mode accounting for measured gas-phase ammonia (Fountoukis & Nenes, 2007) and the organic water was also taken into account (H. Guo et al., 2015). Detailed information can be found in Section S4.

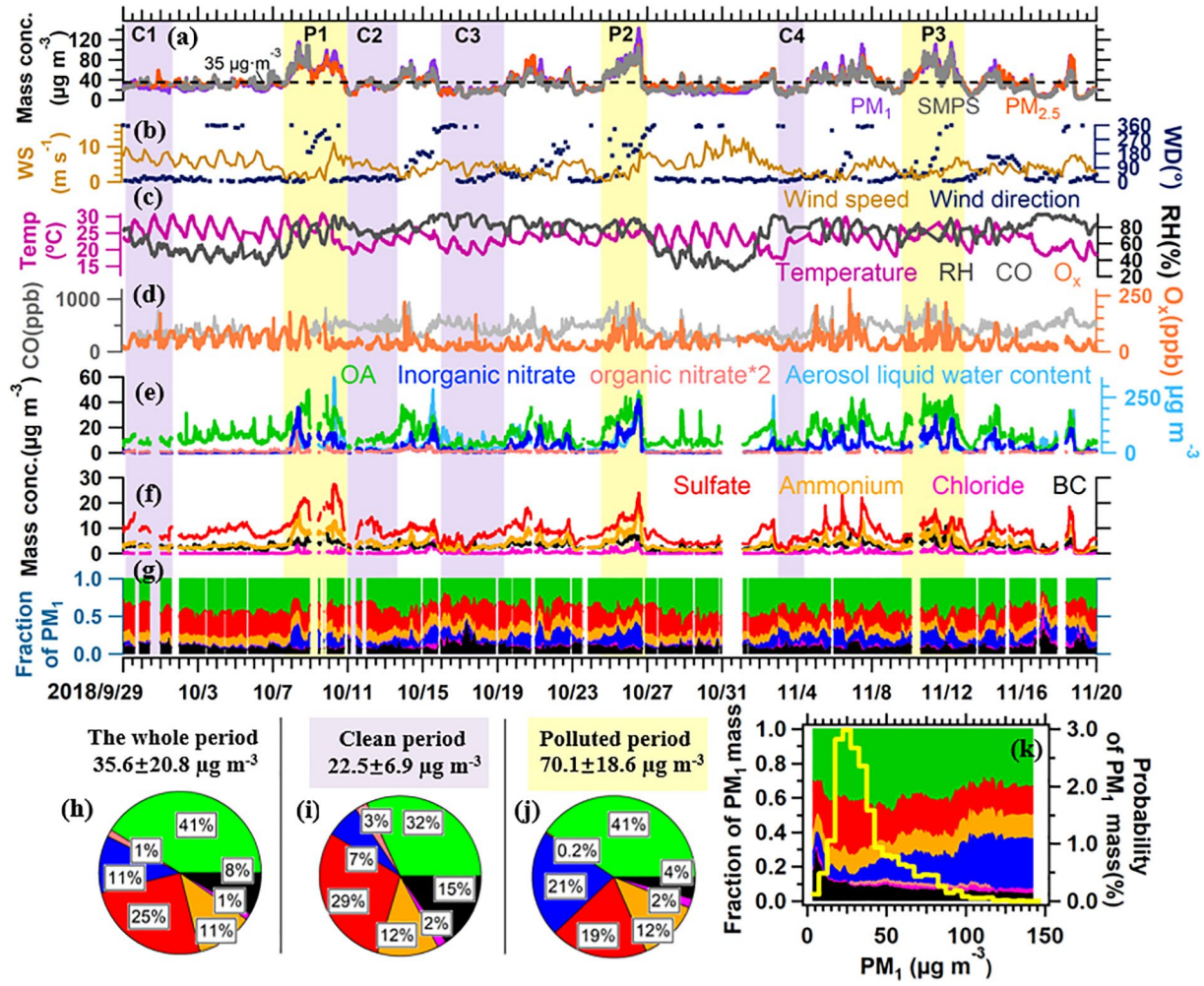

Figure 1. (a) Mass concentrations of total PM_1 obtained from aerosol mass spectrometer and scanning mobility particle sizer, and online $PM_{2.5}$; (b–c) Time series of meteorological parameters including wind speed, wind direction, temperature, relative humidity (RH); (d) Time series of CO and Ox (= O_3+NO_2); (e, f) Time series of main chemical components in PM_1 and aerosol liquid water content (ALWC) calculated based on ISORROPIA model. The organic and inorganic nitrates are resolved based on NO_2^+/NO^+ method (Farmer et al., 2010; Fry et al., 2013), as detailed information shown in Section S3; (g) Time series of mass fraction of each component in total PM_1. The pie charts of the average chemical composition of PM_1 during (h) the whole periods, (i) the clean periods and (j) the polluted periods; (k) Fraction of each component in PM_1 as a function of PM_1 mass concentration. The probability density distribution of PM_1 mass concentration was shown on the right axis. Local time (UTC+8) is used here and also in the following figures.

The ALWC was greatly enhanced during the polluted periods (Figures 1e and S13b), which was mainly driven by the hydrophilic property of inorganic salts, for example, sulfate and inorganic nitrate, as shown in Figure 3a (Colberg et al., 2003; Wu et al., 2018; Xue et al., 2014). When the ALWC was considered in the total PM_1, ALWC (34.1 ± 41.6 μg m^{-3}) could account for 49% of PM_1 mass concentration on average (Figure S13c).

High concentrations of ALWC can provide large surfaces for semi-volatile NH_4NO_3 condensation and N_2O_5 uptake, thus enhance the formation of inorganic nitrate (Bertram & Thornton, 2009; Thornton et al., 2003). The scatter plot of gas-phase NH_3 versus inorganic nitrate shows that when gas-phase ammonia was higher than ~5 μg m^{-3}, the inorganic nitrate concentration did not positively correlate with its precursors but increased as a function of ALWC (Figure 3b). Meanwhile, higher molar ratios of aerosol-phase [inorganic NO_3]/[SO_4] (mole $mole^{-1}$), which increased as a function of ambient RH and ALWC, were also observed (Figures S12b and S12c).

We calculated the time series of pH values based on the estimated liquid H^+ concentration from ISORROPIA-II and ALWC (H. Guo et al., 2015). The average pH in this study was 2.6 ± 0.7, within a range of

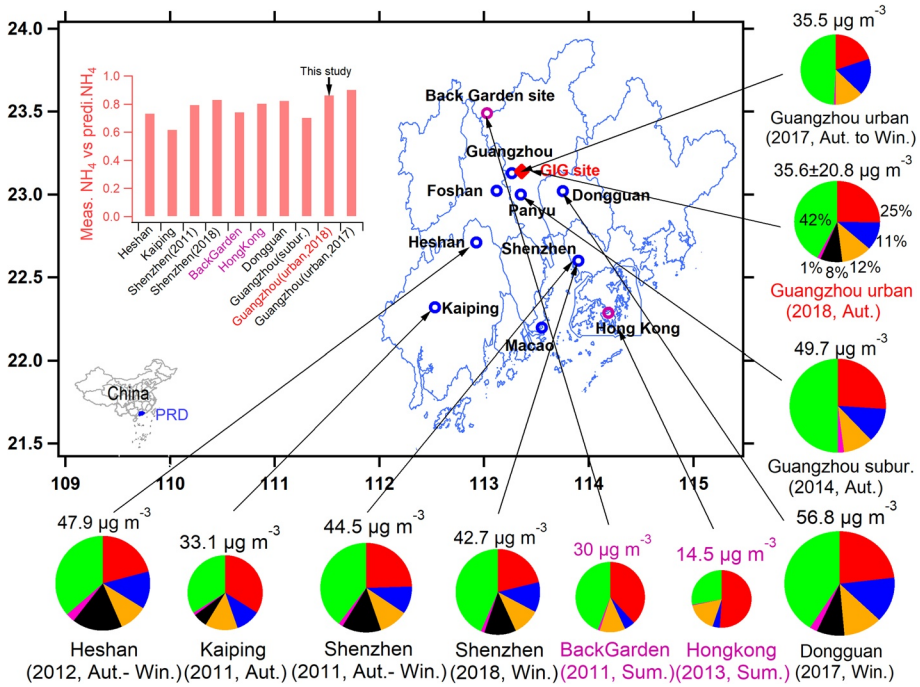

Figure 2. A summary of average chemical compositions of PM_1 measured by aerosol mass spectrometer in the Pearl River Delta (PRD) areas. The inserted plot shows the ratios of measured NH_4 versus predicted NH_4 at each observation site. The ammonium balance ratios suggest the overall aerosols are acidic in the PRD region. For comparison, the organic nitrate masses resolved in this study were added into the total OA masses.

1.1–3.8. As shown in Figure 3c, the gas-particle partitioning of inorganic nitrate is very sensitive to the pH ranges. When pH increased above 3, NH_4NO_3 almost existed as particle phase. Although Figure S12d shows the pH in this study was mainly controlled by the sulfate based on the molar ratio of aerosol-phase $[NO_3]/[2SO_4] < 1$ (H. Guo et al., 2016), a recent study proposed that aerosol pH and its uncertainty were mainly determined by the ambient ALWC when ammonia is abundant (Zheng et al., 2020). Color-coding of sulfate in Figure 3c indeed shows that the variation of sulfate did not impact the pH largely enough to influence gas-particle partitioning of inorganic nitrate substantially.

The interaction of ALWC and pH with inorganic nitrate formation is more complex if considering these processes in a dynamic way. On one hand, the higher ALWC and pH can promote the inorganic nitrate formation, on the other hand the substantially increased inorganic nitrate would also impose positive feedback on ALWC and pH values (Figure 3d), for example, higher inorganic nitrate concentrations would promote more ALWC formation due to its hydrophilicity, while more ALWC would dilute the H^+ and lead to higher pH of aerosols, then favor the gas-phase NH_4NO_3 condense in the aerosol phase. We illustrated these mutual promotion processes in Figure 3d, which provides a co-beneficial control strategy for fine particle concentrations under the polluted periods (Y. Wang, Chen, et al., 2020).

3.3. Size Distributions

The average mass size distribution of total aerosols measured by the AMS shows good agreement with that from the SMPS (Figure 4a), verifying the robustness of size distributions measured here. The aerosol size distributions in the polluted and clean periods are also shown in Figures 4b and 4c. During the polluted periods, the average peaks of size distributions of each species (vacuum aerodynamic size, d_{va} = 600–700 nm) were generally larger than these from the clean periods (d_{va} = 500–600 nm), indicating a faster particle growth rate of aerosols during the haze events. Note that the size peaks of species under $PM_{2.5}$ ranges might be slightly larger than the values shown here due to AMS lens size cut of PM_1 was used here (Elser et al., 2016).

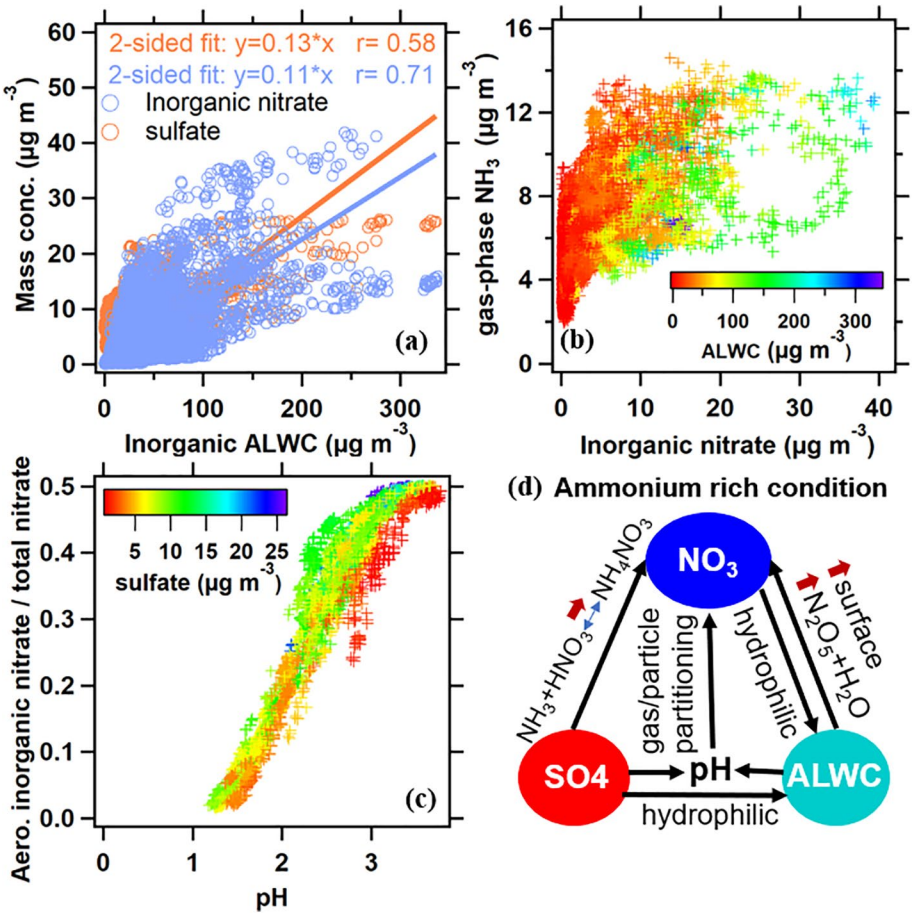

Figure 3. (a) Scatter plots of sulfate and inorganic nitrate versus calculated aerosol liquid water content (ALWC) only based on ISORROPIA model; (b) Scatter plot of gas-phase NH3 versus aerosol-phase inorganic nitrate, which was color-coded by the total ALWC; (c) Fraction of aerosol-phase inorganic nitrate in total nitrate (gas + aerosol phase) as a function of pH. The scatters were color-coded by the sulfate mass concentrations; (d) Schematic plot of the positive feedback among particulate NO_3, SO_4, ALWC and pH.

The similar size distributions of the SIA species (sulfate, ammonium, nitrate) and chloride during the polluted periods suggested a well internally mixed state of these components, which is consistent with what has been observed during the haze events in other urban areas (W. Hu, Hu, Hu, Jimenez, et al., 2016; Y. J. Li, Lee, et al., 2015; Y. Sun et al., 2016). The well mixed state of aerosols in the polluted periods indicates different inorganic species might have been through the similar growth processes, for example, the promoted nitrate formation from increased sulfate mass concentration (as discussed above) and from chloride (Qiu et al., 2019) is probably one of the reasons. During the clean periods, the peak of sulfate size distribution was slightly higher (~580 nm) than those from nitrate and chloride (~520 nm, Figure 4b), implying sulfate might have different origins and/or transformation mechanisms with other species, for example, from cloud chemistry or transportation from other regions (Ge, Seytan, et al., 2012; Ge, Zhang, et al., 2012; W. Hu, Hu, Hu, Jimenez, et al., 2016; Ovadnevaite et al., 2007; Q. Zhang et al., 2005).

Compared to SIA, OA showed extra enhanced mass contributions at d_{va} of 100–400 nm in the both clean and polluted periods, which is consistent with observed results in other urban areas (Allan et al., 2003; Huang et al., 2010; J. Sun et al., 2010, and references therein). The excess mass of OA at smaller d_{va} was probably contributed by the primary sources (i.e., vehicle emissions), which is supported by the similarly enhanced mass of vehicle emission tracer m/z 57 ($C_4H_9^+$ and $C_2H_3O^+$) at the smaller d_{va} (Figure 4e). Meanwhile, the peaking sizes of SOA-tracers m/z 44 (CO_2^+, 550–700 nm) and m/z 43 ($C_3H_7^+$ and $C_2H_3O^+$, ~500–600 nm) are slightly larger than primary tracer m/z 57 (~500 nm), which is consistent with their secondary origins (Ng, Canagaratna, Jimenez, Chhabra, et al., 2011; Yatavelli et al., 2015). The high-resolution ion fitting of

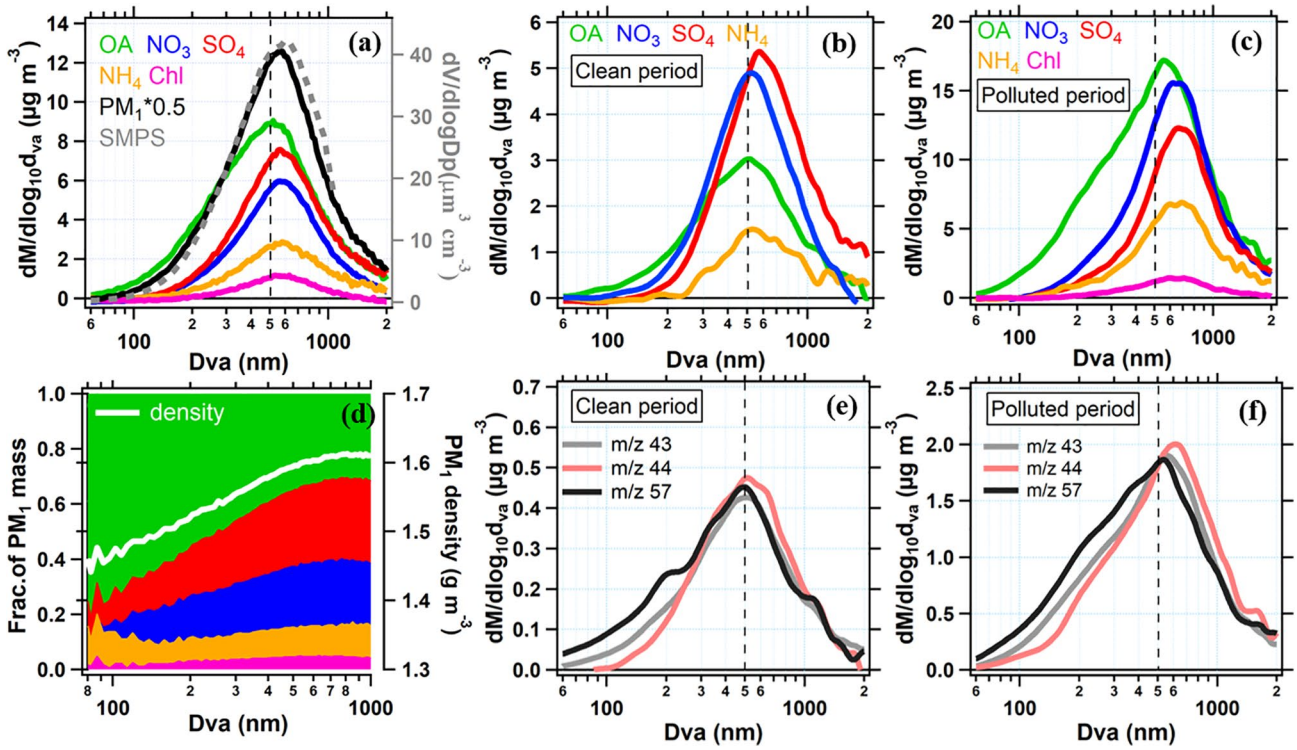

Figure 4. (a) Average size distributions and main components of NR-PM_1 measured by aerosol mass spectrometer and total aerosol size distributions from scanning mobility particle sizer (dashed line). Vacuum aerodynamic sizes (d_{va}) were shown here. Average size distributions of NR-PM_1 species in the (b) clean periods and (c) polluted periods; (d) The fraction of NR-PM_1 species (left axis) and PM_1 density (right axis) as a function of d_{va}; Average size distributions of m/z 43, m/z 44, m/z 57 in the (e) clean periods and (f) polluted periods. The detailed high resolution ion compositions for m/z 44, 43 and 57 can be found in Figure S14. Note the total nitrate size distribution is shown here. Since inorganic nitrate dominated the total nitrate (~88% in average), the total nitrate size distribution should resemble the inorganic nitrate size distribution here.

the UMR m/z 44, 43, and m/z 57 can be found in Figure S14. As the d_{va} increased from 80 nm to 1 μm, the SIA fraction in PM_1 ranged from 20% to 60%, leading to an enhanced PM_1 density from 1.4 to 1.6 g cm^{-3} (BC is not included). The large variation of aerosol chemical compositions as a function of d_{va} highlights the complex sources and formation mechanism of different species.

3.4. Source Apportionment of OA

The five OA factors in this study include three types of POA (28%): nitrogen-containing OA (NOA, 3%), hydrocarbon-like OA (HOA, 16%), cooking OA (COA, 8%), and two types of SOA (72%): low-volatility oxygenated OA (LV-OOA, 45%), and semi-volatile oxygenated OA (SV-OOA, 27%).

3.4.1. NOA

The nitrogen-containing OA (NOA) showed similar prominent nitrogen ions in the spectrum as aliphatic amine, for example, CH_5N^+ (m/z 31), $C_2H_4N^+$ (m/z 42), $C_3H_6N^+$(m/z 56) and $C_3H_8N^+$ (m/z 58) (Aiken et al., 2009; Hayes et al., 2013; Y. L. Sun et al., 2011). NOA only contributed 3% of total OA masses, which is similar to the low contributions of NOA (or called LOA) found in other studies, such as 5% in the Pasadena study (Hayes et al., 2013), 5.8% in the New York City study (Y. L. Sun et al., 2011), and 9% in the Mexico study (Aiken et al., 2009). Auto-correlation plots of OA factors describe their correlations with themselves on different time offsets (Hayes et al., 2013). The auto-correlation curve of NOA in this study is very narrow, suggesting this factor may come from a relatively transient local source (Figure 5f). The peaking time of NOA mass in the diurnal variation was consistent with the morning traffic rush hours (~8:00), indicating it might originate from the emissions of surrounding traffic flows (Figure 5d). It is also supported by the positive correlation between NOA and propene ($R = 0.58$) which emitted from gasoline cars (H. Guo et al., 2011; Hong-li et al., 2017) (Figure S8).

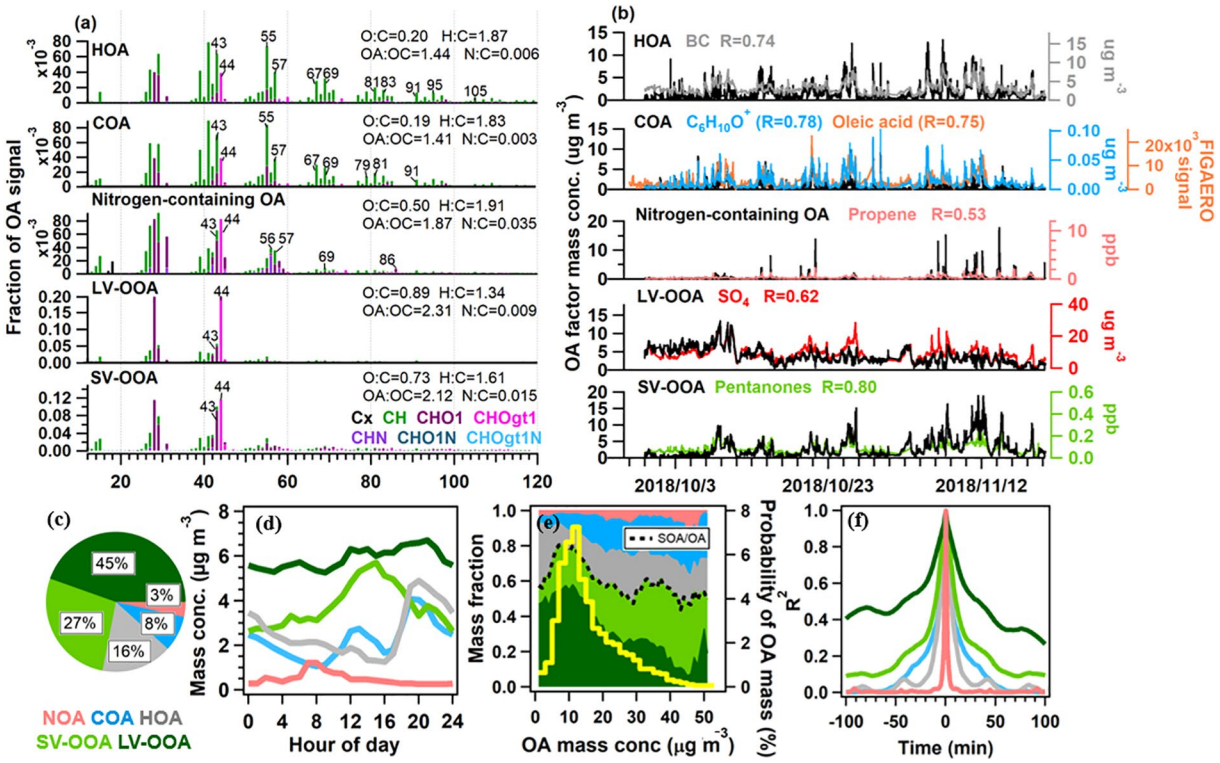

Figure 5. (a) High-resolution spectra and (b) time series of five OA factors: hydrocarbon-like OA (HOA), cooking-emission OA (COA), nitrogen-containing OA (NOA), low-volatility oxygenated OA (LV-OOA), semi-volatile oxygenated OA (SV-OOA). The time series of external tracers for each factor were also shown in panel (b). (c) Pie chart of average OA factor fractions in total OA; (d) Diurnal variations of five OA factors; (e) Diurnal variations of the different OA factor fractions in total OA (left axis). The probability distribution of OA mass concentration was shown on the right axis; (f) The autocorrelation of time series of each OA factor.

3.4.2. HOA

Consistent with the previous studies (Canagaratna et al., 2004; Ng et al., 2010), the spectrum of HOA is dominated by alkyl fragments ($C_nH2_{n+1}^+$ and $C_nH_{2n-1}^+$, Figure 5a). Average O:C of HOA (0.2) in this study is within the range of 0.1–0.5 summarized in HOA from prior studies (Aiken et al., 2008; Canagaratna et al., 2015; Jimenez et al., 2009; Y. J. Li et al., 2017; Zhou et al., 2020).

High correlations were also observed between the time series of HOA with BC ($R = 0.72$), NOx ($R = 0.81$) and propane ($R = 0.88$, Figure S8), supporting the vehicle emission related origins of HOA reported in the previous studies (Docherty et al., 2011; Lanz et al., 2007; Ulbrich et al., 2009; Q. Zhang et al., 2005, and references therein). HOA exhibited slightly enhanced peaks in the morning and prominent peaks during nighttime (18:00 to 21:00) when the traffic jam happened (Figure 5d). Similar variations were also observed in HOA/ΔCO, HOA/BC when excluding atmospheric dilution effects (Figure 6a), supporting the association of HOA with vehicle emissions. The less enhanced morning peak of HOA is probably associated with the separation of NOA factor in PMF solution. The latter contributed a fraction of POA masses from fresh vehicle emissions in the morning, which is supported by the prominent morning and night peaks in the diurnal variation of (NOA + HOA)/BC (Figure 6a).

It is well known that many cities have weekday/weekend effect on air pollutants due to the varied traffic emissions. In downtown areas of Guangzhou, the mass concentrations of primary species including POA (i.e., HOA and COA), BC and NOx were greatly enhanced during the nights of the weekends compared to those at weekdays (Figure 7). The enhancements of primary species during weekends are quite contrary to the observation results in Pasadena where low concentrations of HOA and NOx due to low traffic flows during weekends were found (Hayes et al., 2013). Secondary species and meteorological parameters

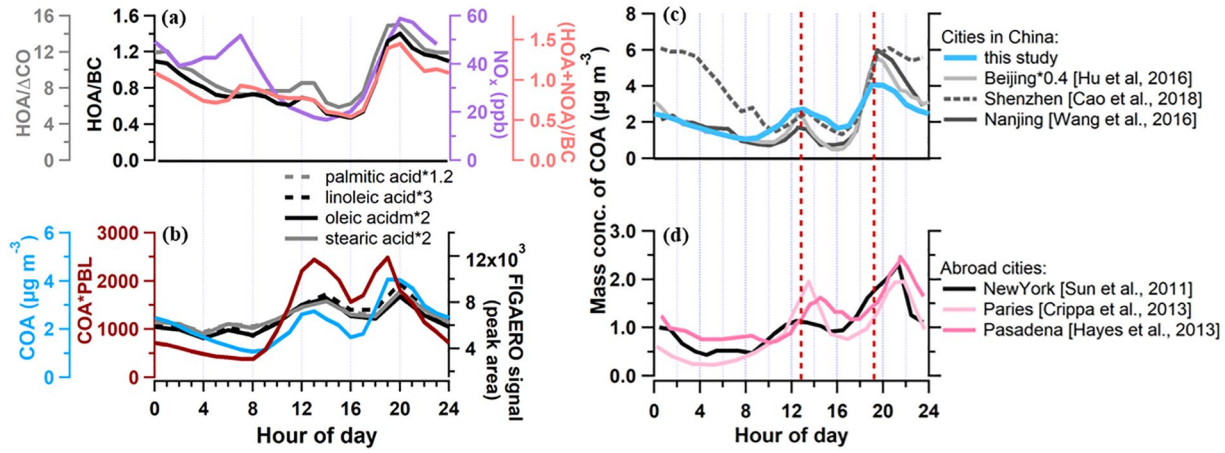

Figure 6. (a) Diurnal variations of hydrocarbon-like organic aerosol (HOA)/ΔCO (ΔCO = CO-background CO), HOA/BC, (HOA + NOA)/BC and NOx. (b) Diurnal variations of cooking organic aerosol (COA) and dilution-corrected COA based on boundary layer height (COA × PBL). Diurnal variations of cooking tracer: four fatty acids including oleic acid ($C_{18}H_{34}O_2$), linoleic acid ($C_{18}H_{32}O_2$), stearic acid ($C_{18}H_{36}O_2$) and palmitic acid ($C_{16}H_{34}O_2$) measured by on-line FEAGEO-CIMS were also shown. Diurnal variations of COA in the (c) Chinese cities (Guangzhou, Beijing, Nanjing, Shenzhen) versus (d) European and US cities (New York, Paris, Pasadena).

showed negligible differences between the weekday/weekend regarding diurnal variations (Figure 7). After investigations, we found the enhanced HOA, BC, and NOx mass concentrations on weekends were probably caused by the high returning traffic flows from suburban or surrounding cities to Guangzhou cities on

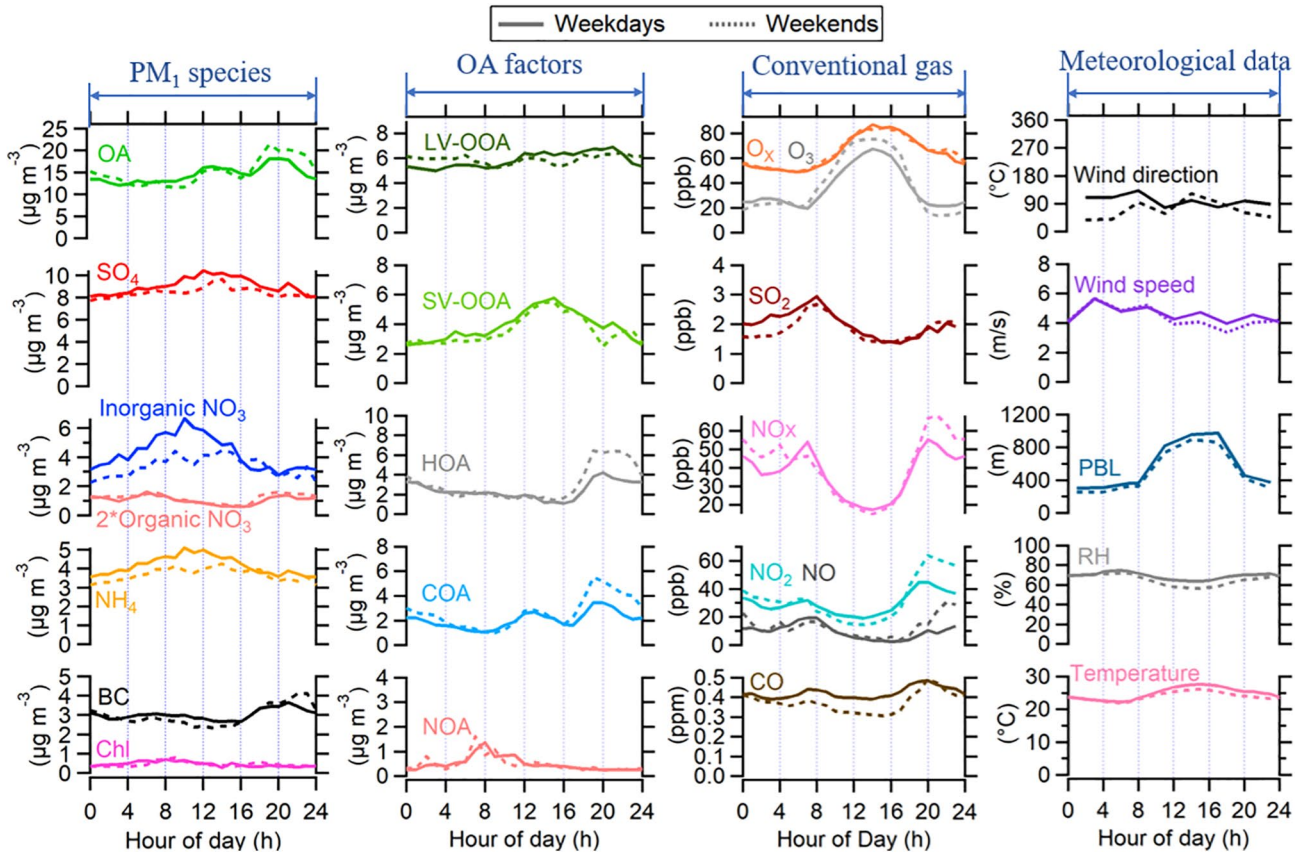

Figure 7. Average diurnal variations of PM_1 chemical components (first column), OA factors (second column), trace gases (third column) and meteorological parameters (fourth column) during weekdays (solid line) and weekends (dashed line).

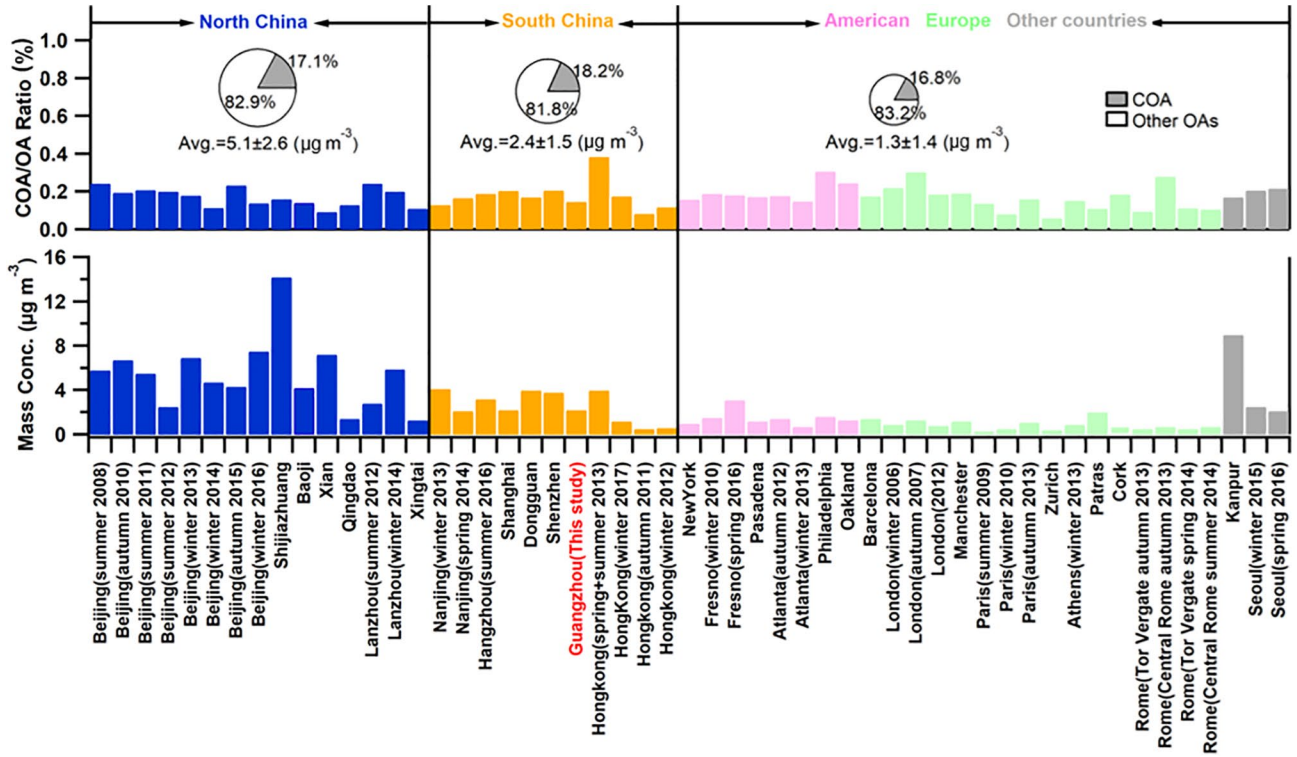

Figure 8. Summary of the cooking organic aerosol (COA) fraction in total OA based on aerosol mass spectrometer measurements. We categorized different studies based on the locations of their observation sites: North China (blue bars), South China (orange bars), American (pink bars), Europe (mint bars) and other cities (gray bars). The three insert pies represented the average COA fraction in total OA corresponding to each category. Note that selected results from Beijing were shown here.

Sunday evenings. The weekday/weekend effects on vehicle-related primary species underscore the important contributions of vehicle emissions to fine particles.

3.4.3. COA

The fatty acids (e.g., oleic acid, linoleic acid, stearic acid, etc.) were reported to be the main quantified organic compounds (~75%) from the residential cooking emissions (Reyes-Villegas et al., 2018; Zhao et al., 2015). In this study, the PMF resolved COA factor based on AMS was compared to these ambient cooking tracers at high time resolution (1 h) for the first time. Generally, COA showed the best correlations with aerosol fatty acids among all the PMF factors, for example, oleic acid ($C_{18}H_{34}O_2$, $R = 0.77$), linoleic acid ($C_{18}H_{32}O_2$, $R = 0.72$), stearic acid ($C_{18}H_{36}O_2$, $R = 0.76$), azelaic acid ($C_9H_{16}O_4$, $R = 0.81$), and palmitic acid ($C_{16}H_{32}O_2$, $R = 0.73$, Figures 5b and S15), supporting the validity of COA resolved here and the finding that COA was mainly composed by cooking oil from frying in urban areas (Reyes-Villegas et al., 2018).

On average, COA accounted for 8% of the total OA at Guangzhou (Figure 5c). Note that although a higher RIE (1.56–3.06) (Katz et al., 2021; Reyes-Villegas et al., 2018) or unit CE of COA instead of 0.5 (Yin et al., 2015) were proposed in other literatures, we did not find a better correlation of the total aerosol masses between SMPS and AMS when such high ranges response factors (RIE x CE = 0.4–5) were applied (Figure S16), which is probably due to the uncertainty of measurement techniques and low COA fraction in total aerosol (8%). Thus, a default RIE of 1.4 and CE of 0.5 for COA were still used here.

COA was widely observed in urban areas all over the world. For comparisons, the COA mass concentrations and fractions in total OA based on the literature results were summarized in Figure 8. In general, the fractions of COA in bulk OA (17%–18% on average) are similar across different regions in the world (for example, Crippa et al., 2013; Kim et al., 2017; Y. Sun et al., 2016; Xu et al., 2014) (Table S2), while COA showed higher mass concentrations in China than these from western countries (for example, W. Li, Liu, et al., 2018; Y. L. Sun et al., 2013; Y. Wang, Wang, et al., 2018; Y. Zhang et al., 2015). The universal high COA

fractions of OA in urban areas indicate cooking is a non-negligible source for non-fossil carbons in urban areas. And the high COA concentrations in China also indicate the cooking emissions needs to be better controlled for improving the air quality in urban areas.

The diurnal variation of COA, as well as the cooking tracer organic fatty acids, showed two enhanced peaks during 12:00–13:00 (2.7 μg m^{-3}) and 19:00–20:00 (4.1 μg m^{-3}), which corresponds to the lunch and dinner time respectively (Figure 6b). The enhanced COA during the weekend night (Figure 7) is probably associated with the enhanced domestic cooking activities. By comparing the diurnal variation of COA with other studies, it is interesting to find that the COA peaking time in China, especially for the dinner peaking time (~20:00) (Cao et al., 2018; W. Hu, Hu, Hu, Jimenez, et al., 2016; J. Wang et al., 2016), is generally 1–2 h earlier than those from the western countries (Figures 6c and 6d) (Crippa et al., 2013; Hayes et al., 2013; Y. L. Sun et al., 2011). The peaking time differences are probably caused by the different lifestyle in different countries.

3.4.4. SV-OOA and LV-OOA

Both the LV-OOA and SV-OOA are distinguished by the prominent ions of *m/z* 44 (CO_2^+) and *m/z* 28 (CO^+). The LV-OOA showed the highest O:C ratios of all factors (0.89), and then followed by SV-OOA of 0.73. The O:C ratios of both factors are within the range of 0.64–1.15 reported in the diverse OOA factors from the previous studies (Aiken et al., 2008; Jimenez et al., 2009; Ng, Canagaratna, Jimenez, Chhabra, et al., 2011; Zhou et al., 2020). Good correlations are found between LV-OOA and sulfate ($R = 0.64$), as well as acetone (C_3H_6O, $R = 0.54$, Figure S8) (Aiken et al., 2009; Huang et al., 2010; Q. Zhang et al., 2007, and references therein). The long lifetime of sulfate and acetone (~a few days) supports the LV-OOA was relatively aged in ambient air and strongly influenced by regional transport (Hayes et al., 2013; Lanz et al., 2007).

The diurnal variation of SV-OOA peaked around 12:00–14:00 of noontime despite the expanded boundary layer, suggesting SV-OOA was freshly produced from the photochemical process and is similar to the SV-OOA found in other studies (Y. L. Sun et al., 2011; J. Zhang, Liu, et al., 2013; Q. J. Zhang, Beekmann, et al., 2013). Good correlations were found between SV-OOA and VOC photochemical oxidation products like pentanone ($R = 0.70$) (Figure S8). Based on the same campaign, C. Wang, Yuan, et al. (2020) found the oxidation from long-chain alkanes (C_8-C_{20}) and aromatics can explain ~35% of the fresh SOA formation during noontime.

We compared our OA factors results with other studies conducted in the PRD regions in Figure S17. It showed that the SOA can account for 43%–78% of the OA masses in different areas of the PRD, with ~60% for urban areas and ~73% for downwind sites in average. The result that higher SOA fractions in downwind areas than in cities is similar to the trend found in the global data set (urban 65% to suburban 83%) (Q. Zhang et al., 2007). The increasing trend of the OOA fraction is mainly due to a longer aging time of OA and/or less primary emission contributions to OA at downwind sites (DeCarlo et al., 2010; Jimenez et al., 2009).

3.5. The Photochemical Oxidation Evolution of OA

In this section, the SOA formation as a function of photochemical age was explored, as shown in Figure 9. The atmospheric dilution effect of OA can be ignored when normalizing OA and OA factors with ΔCO (= relative change between ambient CO and background CO of 125 ppb, Figure S18). The photochemical age was calculated by the ratio of *m* + *p*-xylene to ethylbenzene with different k_{OH}, leading to different lifetime in the atmosphere (de Gouw, Middlebrook, et al., 2005; de Gouw, Warnekea, et al., 2005; Y. Wang, Yuan, et al., 2020; Wu et al., 2020), and the detailed calculation process can be found in Section S5. For comparison with previous studies, an average ambient OH concentration of 1.5×10^6 molecule cm^{-3} was assumed here. Similar to the prior studies (DeCarlo et al., 2010; Hayes et al., 2013; W. W. Hu et al., 2013; Nault et al., 2018; Schroder et al., 2018), OA/ΔCO increased as a function of photochemical age at a slope of ~2.7 μg m^{-3} h^{-1} (Figure 9a), which is lower than the findings in the Seoul urban plumes by aircraft measurements (Nault et al., 2018), however higher than the results from Beijing (W. Hu, Hu, Hu, Jimenez, et al., 2016) and Chinese outflows measured at a receptor site of NCP (W. W. Hu et al., 2013). When the photochemical age was above 7 h, the OA/ΔCO enhancement rate increased fast, which is similar to the observations in Los Angeles and Mexico City (2–5 μg m^{-3} h^{-1}) (Dzepina et al., 2009; Hayes et al., 2013). The averaged OA/ΔCO ratios as a function of photochemical age during the day and night are shown in Figure S19. Consistent

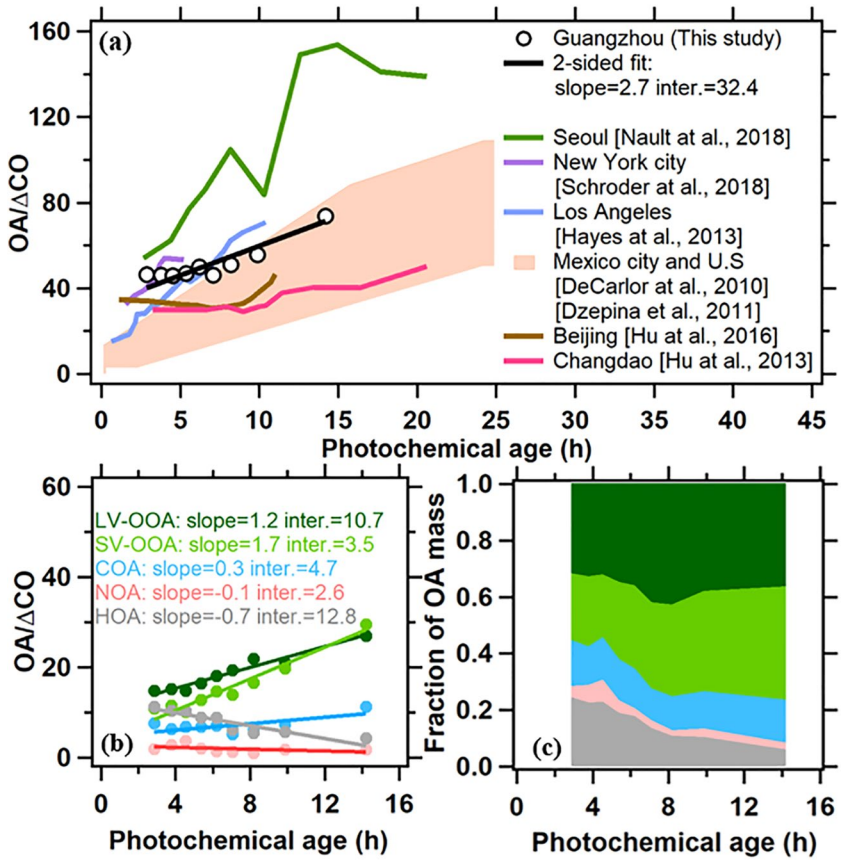

Figure 9. (a) Ambient OA/ΔCO as a function of photochemical age; ΔCO = ambient CO-background CO. Background CO of 125 ppb was applied here (Figure S18). Results from other literature results were also shown. Orthogonal distance linear regression was applied here and in the following. (b) Different OA factors/ΔCO as a function of photochemical age. (c) Mass fractions of OA factors in total OA as a function of photochemical age.

increase of OA/ΔCO between the campaign average and the daytime average versus photochemical age was found, indicating the daytime chemistry dominated the total OA/ΔCO evolution. The OA/ΔCO during nighttime shows negligible variation with photochemical age. It is mainly due to the low OH concentrations in the night leading to the inefficient chemical transformation for VOCs species (de Gouw et al., 2017). The different OA factors/ΔCO and its fraction of total OA as a function of photochemical age were further investigated in Figures 9b and 9c. The fast increase of OA versus photochemical age was mainly contributed by SV-OOA (slope = 1.7 μg m^{-3} h^{-1}) and LV-OOA (slope = 1.2 μg m^{-3} h^{-1}), indicating the SOA, especially the freshly formed SV-OOA produced rapidly within the short timescale (<14 h) of photochemical aging process. During this process, vehicle emission-related HOA/ΔCO decreased rapidly (slope = −0.7 μg m^{-3} h^{-1}, HOA fraction of OA from 24% to 6%) with the enhanced photochemical age, while COA/ΔCO (slope = 0.3 μg m^{-3} h^{-1}, COA fraction of OA ~14%) and NOA/ΔCO (slope = −0.1 μg m^{-3} h^{-1}, NOA fraction of OA ~4%) show much less variation (Figures 9b and 9c). The fast decrease of HOA/ΔCO as a function of photochemical age is consistent with the finding that freshly emitted HOA in the ambient air would undergo dilution with the background air masses and/or be oxidized to produce SOA efficiently due to its semi-volatile properties (Cappa & Jimenez, 2010). The slightly changed COA/ΔCO also agrees with a much lower volatility distribution for COA than HOA in ambient air (Buonanno et al., 2011; Cao et al., 2018).

The intercept of POA (=HOA + COA + NOA)/ΔCO was 16 μg m^{-3} ppm^{-1} when photochemical age was zero, which was in the range of 2–23 μg m^{-3} ppm^{-1} reported in urban areas (De Gouw & Jimenez, 2009; DeCarlo et al., 2010; Hayes et al., 2013; Nault et al., 2018). The emission ratio of POA versus CO was around 15 μg m^{-3} ppm^{-1} if COA was excluded (Figure S20a). The emission ratio between POA and BC is around 10 (Figure S20b).

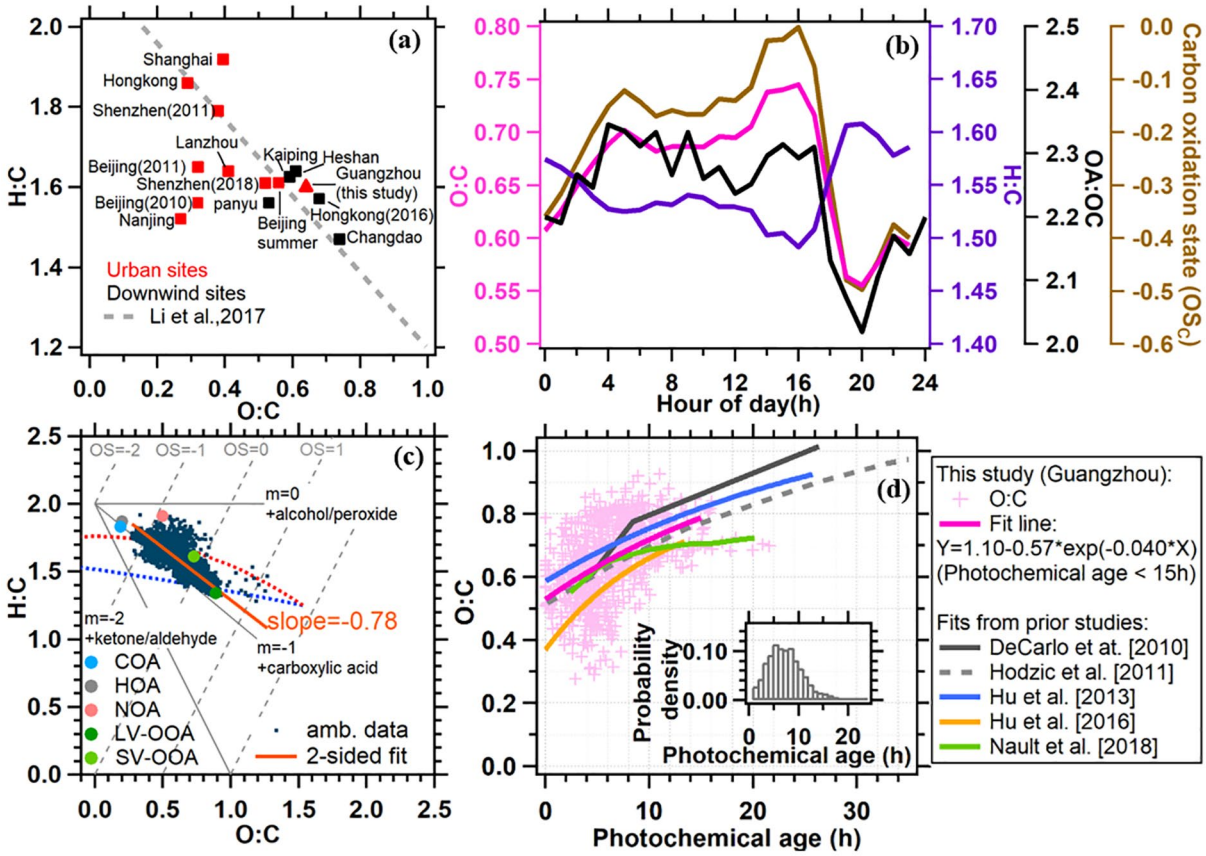

Figure 10. (a) Van Krevelen plots for OA of urban and downwind sites in China; (b) Diurnal profiles of O:C, H:C, OA:OC and carbon oxidation state OSc (= 2 × O:C–H:C) (Kroll et al., 2011) in this study; (c) Van Krevelen diagram for ambient OA and OA factors. A regression slope of −0.78 was shown. (d) O:C ratio of OA as a function of photochemical age in this study. Prior results from several other field measurements were also shown. The O:C in Hodzic and Jimenez (2011), Dzepina et al. (2011), and Hu et al. (2013) were corrected to IA method by multiplying a factor of 1.28. The insert is the probability distribution plot for photochemical age. To avoid fitting bias at higher photochemical age, we fitted the O:C versus photochemical age when the photochemical age is below 15 h.

3.6. Elemental Compositions of OA

Figure 10a shows the comparison of average O:C (0.6 ± 0.1) and H:C (1.6 ± 0.1) in this study with other studies from China based on the updated IA calibrations in Canagaratna et al. (2015). The O:C ratio in Guangzhou was generally at the higher end of O:C ranges reported in urban areas of China (0.3–0.65) (W. Hu, Hu, Hu, Jimenez, et al., 2016; Huang et al., 2010; Y. J. Li, Lee, et al., 2015; Xu et al., 2014, and references therein), and was comparable to the O:C ratios at the downwind urban sites (0.59–0.74) (Gong et al., 2012; W. W. Hu et al., 2013; Huang et al., 2011). The high O:C of OA suggests the OA in Guangzhou city was fairly oxidized, which is consistent with the dominance of SOA in total OA (72%) obtained in this study.

The diurnal variation of the O:C ratio was higher during the daytime than that at night, while the H:C ratio showed the opposite trend due to the replacement of alkyl ions by oxidized ions containing O elements (Figure 10b) (Aiken et al., 2008; Heald et al., 2010). The increase of the O:C ratio from 0.6 to 0.7 in the afternoon was mainly caused by the enhanced SV-OOA formation through the strong photochemical oxidation during this period (Figure 5d). The enhancements of H:C ratio during rush hour and noontime were mainly associated with the primary emissions from cooking and traffic within these time intervals. Average carbon oxidation state (OS_C = 2 × O:C–H:C) (Kroll et al., 2011), displaying a similar diurnal variation as O:C, was approximately in the range of −0.5 to 0.

Van Krevelen plot, shown as H:C versus O:C, was usually used to depict OA aging which involves the processes of oxidation, volatilization, condensation, and dilution in ambient air (Q. Chen et al., 2015; Heald

et al., 2010; Ng, Canagaratna, Jimenez, Chhabra, et al., 2011). In this study, the evolution of O:C and H:C followed along a line with a slope of −0.78 (Figure 10c), which is between the slopes representing the carboxylic acids addition with fragments (−0.5) and carboxylic acid addition without fragmentation or alcohol + carbonyl addition on different carbons (−1) (Heald et al., 2010; Ng, Canagaratna, Jimenez, Chhabra, et al., 2011). This regression slope of ambient OA is within the statistical range of slopes (−0.6 to −0.8) in most urban areas in China (Y. J. Li et al., 2017). The O:C versus H:C from OA factors also evolved along the regression line and exhibited a similar oxidation pathway as the ambient data (Figure 10c).

For a further investigation on OA evolution, the correlation between the O:C ratio and photochemical age is shown in Figure 10d, along with other previous studies (DeCarlo et al., 2010; Hodzic & Jimenez, 2011; W. Hu, Hu, Hu, Jimenez, et al., 2016; W. W. Hu et al., 2013; Nault et al., 2018). The O:C in Guangzhou increased rapidly as photochemical age was higher (<1 day), suggesting a very fast oxidation process of OA in the ambient air. The evolution pathway of OA shown here is nearly identical to the Mexico City observation and Seoul aircraft results when the photochemical age is >∼0.5 days. The scatter plot between O:C and photochemical age can be fitted to an equation as: O:C = a–b × exp (c × age) when assuming bulk OA reactions are first-order process proportional to OH radicals, then the reaction rate coefficient with OH radicals (k_{OH}) can be roughly determined based on the ratio of fitted parameter c with average OH radicals concentration in the ambient air (DeCarlo et al., 2010; W. W. Hu et al., 2013). Finally, k_{OH} was estimated to be 7.4×10^{-12} cm^3 molecules^{-1} s^{-1}, which is in the range of values ($0.3–1.25 \times 10^{-11}$ cm^3 molecules^{-1} s^{-1}) reported in other anthropogenic influenced areas (Hodzic & Jimenez, 2011; Spracklen et al., 2011).

3.7. Determination on Heterogeneous Reaction Rate With OFR

The heterogeneous reaction of bulk OA was investigated by sampling ambient OA into the OFR. As the OH equivalent aging time in OFR varied from several hours to several weeks in OFR when gas-phase VOCs was removed with charcoal denuder (Decemeber 6 to December 12), we barely observed OA decay in the OFR (Figure 11a), suggesting a very slow heterogeneous reaction rate of ambient OA with OH radicals (George & Abbatt, 2010; Kroll et al., 2015). Due to the small decrease of total OA, there might be large uncertainties for the heterogeneous reaction rate coefficient ($k_{OH,heteo}$) estimation if such a decay is fitted. Thus, we furtherly investigated the decays of primary species of HOA and COA in the OFR, which were obtained with the entire campaign data set, and were suitable for heterogeneous reaction analysis since secondary HOA and COA formation can be ignored during the short residence time in OFR (160 s).

Making use of a raw OA mass spectral matrix from OFR, the HOA and COA in OFR were obtained by constraining ambient HOA and COA PMF spectra (W. Hu, Hu, Hu, Jimenez, et al., 2016) in ME-2 with a value = 0. The mass fraction of HOA in OFR decreases substantially as OH exposure increases (Figure 11a), while COA showed enhancement at ages <4 days (Figure 11b), which might be influenced by uncertainty from PMF analysis. Thus, we further explored the decay of COA tracer $C_6H_{10}O^+$ ion (Y. L. Sun et al., 2011) and HOA tracer $C_4H_9^+$ ion (Ng, Canagaratna, Jimenez, Zhang, et al., 2011) in Figure 11. Continuous decay of $C_6H_{10}O^+$ and $C_4H_9^+$ ions as a function of OH exposure was observed in OFR. In the following, we will use $C_6H_{10}O^+$ decay as the representative for COA in OFR.

There might be two processes leading to the HOA and COA decays in OFR. One is chemical oxidation and/or fragmentation caused by the heterogeneous reaction of OH radicals, the other is evaporation due to the fast removal of gas-phase equilibrated species oxidized by OH radicals. Since HOA has higher volatility, which might lead to its evaporation during the aging process in OFR (Cappa & Jimenez, 2010). Thus, the HOA decay here represents the upper limit for loss from heterogeneous reactions. Similar assumption is also applicable to COA tracer although it is supposed to have a lower volatility than HOA (Cao et al., 2018; Takhar et al., 2019).

By fitting the HOA and COA tracer ($C_6H_{10}O^+$ ion) decay processes, an upper limit of $k_{OH,heteo}$ was estimated to be 5.4×10^{-13} and 4.0×10^{-13} cm^3 molecule^{-1} s^{-1}, respectively, which is equivalent to lifetime of 14 and 19 days by assuming an average OH concentration of 1.5×10^6 molecule cm^{-3} in ambient air. Similar $k_{OH,heteo}$ (4.0×10^{-13} cm^3 molecule^{-1}) was obtained based on the HOA tracer $C_4H_9^+$ ion. The estimated $k_{OH,heteo}$ is in the lower range of $k_{OH,heteo}$ based on laboratory-generated motor oil OA (4×10^{-13}-3.4×10^{-11} cm^3 molecule^{-1} s^{-1}) (Isaacman et al., 2012; Weitkamp et al., 2008), however, is comparable or slightly higher than the

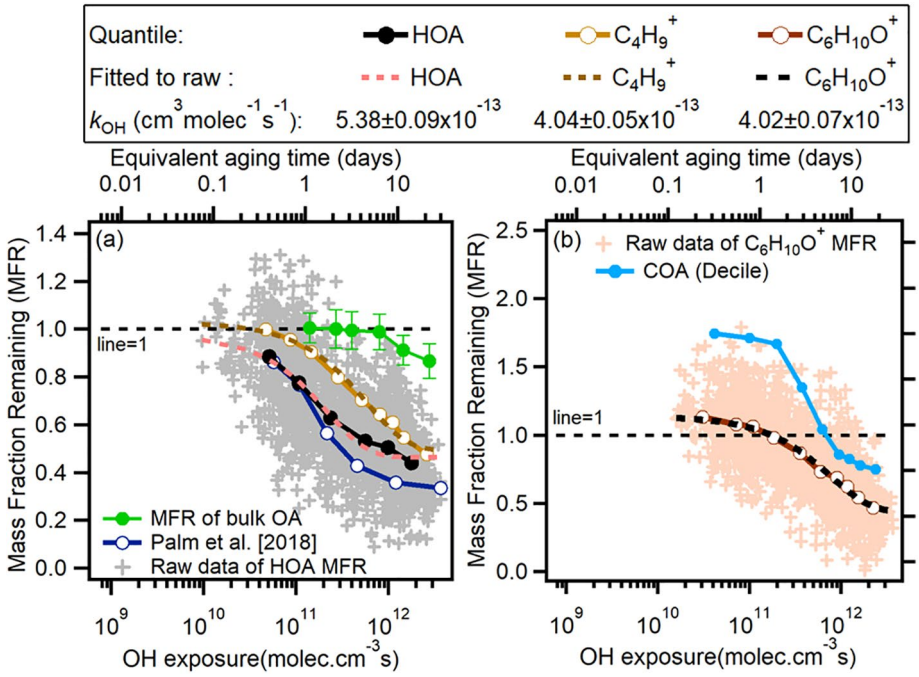

Figure 11. Mass fraction remaining (MFR) of (a) bulk OA, hydrocarbon-like organic aerosol (HOA), $C_4H_9^+$ ions (HOA tracer) as a function of OH exposure. The MFR = C_i / C_0 were calculated based on species mass concentration in OFR output (C_i) versus these in ambient air (C_0). The HOA decay results obtained from Amazon forest areas based on Palm et al. (2018) was also shown; (b) MFR of cooking organic aerosol (COA) and $C_6H_{10}O^+$ ion (COA tracer) in OFR output as a function of OH exposure. We fitted the decay based the equation of $C_i / C_0 = e^{-k_{OH} \times OH_{exp}}$, where k_{OH} is the heterogeneous reaction rate coefficient between species C and OH radicals. OH_{exp} is the OH exposure estimated in OFR. Quantile here is referred to the averaged values from continuous intervals by dividing the number of datapoints into user-defined equal probabilities.

ambient OA from field studies using OFR (1.5–4.0 × 10^{-13} cm^3 molecule^{-1} s^{-1}) (W. Hu, Palm, et al., 2016; Ortega et al., 2016). The long heterogeneous lifetime of HOA and COA (~2 weeks) is consistent with that of ambient isoprene-derived SOA (~19 days) obtained in the southeastern United States and amazon forest areas using a similar estimation method with OFR, and slightly less than the OA lifetime estimated from Los Angeles (~50 days) by fitting the total OA/ΔCO versus photochemical age in OFR. The generally lower $k_{OH,heteo}$ of ambient OA compared with the laboratory generated OA emphasizes the more oxidized and complicated state of ambient OA than the laboratory-generated aerosols, underscoring the importance to investigate atmospheric processes under ambient conditions. Within the ambient RH range of 40%–100%, we found negligible influences of RH to the decay of HOA and the COA tracer ($C_6H_{10}O^+$) as a function of OH exposure, as shown in Figure S21. It is consistent with the finding that when ambient RH is above 50%, the ambient particles were general liquid based on particle bounce measurements in other Chinese megacities (Bateman et al., 2015; T. Liu, Zhou, et al., 2019; Y. Liu, Wu, et al., 2019). Thus, the kinetic limitations for OH uptake due to slow diffusion in ambient OA should be negligible (Y. J. Li, Liu, et al., 2015; Pajunoja et al., 2016).

Based on $k_{OH,heteo}$ discussed above, an effective reactive uptake coefficient of OH radical (γ_{OH}) on ambient OA can be estimated in the following equation (Smith et al., 2009):

$$\gamma = \frac{4 \cdot k_{OH} \cdot V_{OA} \cdot \rho_0 \cdot N_A}{c \cdot S_{OA} \cdot MW_{OA}}$$

where the k_{OH} is the heterogeneous reaction rate coefficient of OA. V_{OA} and S_{OA} are the aerosol volume and aerosol surface area, respectively. The ratio of V_{OA}/S_{OA}, which can be obtained from SMPS, is calculated as 0.054 × 10^{-6} m in this study. MW_{OA} is the molar mass of OA. Here we assuming the molar masses of both HOA and COA are 170 g mol^{-1} (Smith et al., 2009). ρ_0 is the aerosol density of in OFR (1.59 ± 0.09 g cm^{-3}).

c is the mean speed of gas-phase OH radicals, calculated as $(8\ RT = \pi M)^{0.5}$. c = 604 m s^{-1} (T = 293 K) was estimated here. N_A is the Avogadro's number. More detailed information on this calculation also can be found in Section S6 and Table S3.

The final estimated γ_{OH} based on HOA and COA tracer decay was 0.84 and 0.76, respectively, which are generally consistent with the γ_{OH} obtained using the ambient isoprene-derived SOA in OFR (0.59–0.68) and in the range of γ_{OH} from the motor oil OA (0.72–8) and cooking tracer palmitic acid (0.8–1) (Isaacman et al., 2012; McNeill et al., 2008). The high γ_{OH} obtained here suggests the OH radicals can be efficiently taken up on the ambient particle surfaces in the urban plumes.

4. Conclusions

The real-time compositions, size distributions and aging processes of submicron aerosol (PM_1) were systematically investigated in urban area of Guangzhou during the autumn (October–November) of 2018. The average mass concentration of PM_1 during the campaign was 35.6 ± 20.8 μg m^{-3}, which was mainly contributed by OA (42%), then followed by sulfate (25%) and inorganic nitrate (11%). Consistent with the previous studies, the inorganic nitrate was found to be the main contributor for the enhancement of fine particles (40%–50%) during the polluted periods in Guangzhou autumn. In addition to adverse meteorology conditions (e.g., shallow boundary layer), the fast increase of nitrate formation during the polluted periods was not only due to higher precursor concentrations of nitrate (such as NO_2, N_2O_5, NH_3), but also through the positive feedback from higher sulfate, ALWC and pH values. The promotion effect among nitrate, sulfate, ALWC, and pH suggests that the cooperative control of multiple components is necessary for solving the haze formation.

Source apportionment results showed the ambient OA in Guangzhou autumn was comprised of primary vehicle emission related OA: NOA (NOA, 3%), HOA (16%), and cooking emission related COA (8%), as well as freshly formed SOA (SV-OOA, 27%) and aged-SOA (LV-OOA, 45%). The weekday/weekend effects showed substantially enhanced HOA and COA during weekend nights, which might be associated with the increased returning traffic flows from surrounding areas and increased household cooking activities. The COA fractions in total OA (17%–18% in average) are generally similar among different regions, suggesting cooking is a non-negligible non-fossil source in urban areas across the world, and shall be seriously considered in the policy-making for the fine particle control.

The dominance of SOA in total OA in Guangzhou autumn led to a high OA oxidation state (O:C = 0.6 ± 0.1, H:C = 1.6 ± 0.1, OS_C = −0.3 ± 0.1). The OA/ΔCO increase as a function of photochemical age with the dominant contributions from SV-OOA and LV-OOA. The aging process of OA was further investigated with a field-deployed OFR based on OH chemistry. By fitting the continuous decays of HOA and COA tracer versus OH exposure in OFR, the upper heterogeneous oxidation reaction rate ($k_{OH,heteo}$ = 4.0–5.4 × 10^{-13} cm^3 $molecules^{-1}$ s^{-1}) was obtained, which is equivalent to more than 2 weeks of heterogeneous lifetime of ambient OA. The $k_{OH,heteo}$ obtained across different types of OA species is one magnitude lower than the bulk k_{OH} estimated based on fitting the ambient O:C with photochemical age (7.4 × 10^{-12} cm^3 $molecule^{-1}$ s^{-1}), indicating gas-phase oxidation played an important role during ambient OA aging processes and the heterogeneous oxidation pathway was not the main sink for ambient OA. Finally, the γ_{OH} was estimated based on the calculated $k_{OH,heteo}$. The high γ_{OH} with 0.84 of HOA and 0.76 of COA underscore the efficient uptake of OH radicals on ambient OA.

Conflict of Interest

Francesco Canonaco, is employed by Datalystica Ltd., the official distributor of the SoFi Pro licenses.

Data Availability Statement

The data set used to evaluate the conclusions in the study is available at https://data.mendeley.com/datasets/tkfrmhh5jc/1.

Acknowledgments
This work was supported by National Natural Science Foundation of China (grant No. 41875156, 41773114), Natural Science Foundation of Guangdong Province (grant No. 2019A1515011153), Guangdong Pearl River Talents Program (2019QN01L948), Guangdong Foundation for Program of Science and Technology Research (Grant No. 2020B1212060053), Guangdong Foundation for Program of Science and Technology Research (Grant No. 2020B1212060053, 2017B030314057), State Key Laboratory of Organic Geochemistry, GIGCAS (SKLOG2020-5, SKLOG2020-6). Bin Yuan was supported by the National Key R&D Plan of China (grant No. 2019YFE0106300), the National Natural Science Foundation of China (grant No. 41877302), Guangdong Natural Science Funds for Distinguished Young Scholar (grant No. 2018B030306037), and Guangdong Innovative and Entrepreneurial Research Team Program (grant No. 2016ZT06N263).

References

Aiken, A. C., DeCarlo, P. F., Kroll, J. H., Worsnop, D. R., Huffman, J. A., Docherty, K. S., et al. (2008). O/C and OM/OC ratios of primary, secondary, and ambient organic aerosols with high-resolution time-of-flight aerosol mass spectrometry. *Environmental Science & Technology*, *42*(12), 4478. https://doi.org/10.1021/es703009q

Aiken, A. C., Salcedo, D., Cubison, M. J., Huffman, J. A., DeCarlo, P. F., Ulbrich, I. M., et al. (2009). Mexico City aerosol analysis during MILAGRO using high resolution aerosol mass spectrometry at the urban supersite (T0)—Part 1: Fine particle composition and organic source apportionment. *Atmospheric Chemistry and Physics*, *9*(17), 6633–6653. https://doi.org/10.5194/acp-9-6633-2009

Allan, J. D., Alfarra, M. R., Bower, K. N., Williams, P. I., Gallagher, M. W., Jimenez, J. L., et al. (2003). Quantitative sampling using an Aerodyne aerosol mass spectrometer 2. Measurements of fine particulate chemical composition in two U.K. cities. *Journal of Geophysical Research*, *108*(D3). https://doi.org/10.1029/2002JD002359

Bateman, A. P., Gong, Z., Liu, P., Sato, B., Cirino, G., Zhang, Y., et al. (2015). Sub-micrometre particulate matter is primarily in liquid form over Amazon rainforest. *Nature Geoscience*, *9*(1), 34–37. https://doi.org/10.1038/ngeo2599

Bertram, T. H., & Thornton, J. A. (2009). Toward a general parameterization of N2O5 reactivity on aqueous particles: The competing effects of particle liquid water, nitrate and chloride. *Atmospheric Chemistry and Physics*, *9*(21), 8351–8363. https://doi.org/10.5194/acp-9-8351-2009

Buonanno, G., Johnson, G., Morawska, L., & Stabile, L. (2011). Volatility characterization of cooking-generated aerosol particles. *Aerosol Science and Technology*, *45*(9), 1069–1077. https://doi.org/10.1080/02786826.2011.580797

Burkholder, J. B., Abbatt, J. P. D., Barnes, I., Roberts, J. M., Melamed, M. L., Ammann, M., et al. (2017). The essential role for laboratory studies in atmospheric chemistry. *Environmental Science & Technology*, *51*(5), 2519–2528. https://doi.org/10.1021/acs.est.6b04947

Cai, M., Tan, H., Chan, C. K., Mochida, M., Hatakeyama, S., Kondo, Y., et al. (2017). Comparison of aerosol hygroscopcity, volatility, and chemical composition between a suburban site in the Pearl River Delta region and a marine site in Okinawa. *Aerosol and Air Quality Research*, *17*(12), 3194–3208. https://doi.org/10.4209/aaqr.2017.01.0020

Canagaratna, M. R., Jayne, J. T., Ghertner, D. A., Herndon, S., Shi, Q., Jimenez, J. L., et al. (2004). Chase studies of particulate emissions from in-use New York City vehicles. *Aerosol Science and Technology*, *38*(6), 555–573. https://doi.org/10.1080/02786820490465504

Canagaratna, M. R., Jayne, J. T., Jimenez, J. L., Allan, J. D., Alfarra, M. R., Zhang, Q., et al. (2007). Chemical and microphysical characterization of ambient aerosols with the aerodyne aerosol mass spectrometer. *Mass Spectrometry Reviews*, *26*(2), 185–222. https://doi.org/10.1002/mas.20115

Canagaratna, M. R., Jimenez, J. L., Kroll, J. H., Chen, Q., Kessler, S. H., Massoli, P., et al. (2015). Elemental ratio measurements of organic compounds using aerosol mass spectrometry: Characterization, improved calibration, and implications. *Atmospheric Chemistry and Physics*, *15*(1), 253–272. https://doi.org/10.5194/acp-15-253-2015

Canonaco, F., Crippa, M., Slowik, J. G., Baltensperger, U., & Prevot, A. S. H. (2013). SoFi, an IGOR-based interface for the efficient use of the generalized multilinear engine (ME-2) for the source apportionment: ME-2 application to aerosol mass spectrometer data. *Atmospheric Measurement Techniques*, *6*(12), 3649–3661. https://doi.org/10.5194/amt-6-3649-2013

Cao, L.-M., Huang, X.-F., Li, Y.-Y., Hu, M., & He, L.-Y. (2018). Volatility measurement of atmospheric submicron aerosols in an urban atmosphere in southern China. *Atmospheric Chemistry and Physics*, *18*(3), 1729–1743. https://doi.org/10.5194/acp-18-1729-2018

Cappa, C. D., & Jimenez, J. L. (2010). Quantitative estimates of the volatility of ambient organic aerosol. *Atmospheric Chemistry and Physics*, *10*, 5409–5424. https://doi.org/10.5194/acp-10-5409-2010

Chan, C. K., & Yao, X. (2008). Air pollution in mega cities in China. *Atmospheric Environment*, *42*(1), 1–42. https://doi.org/10.1016/j.atmosenv.2007.09.003

Chen, H., Huo, J., Fu, Q., Duan, Y., Xiao, H., & Chen, J. (2020). Impact of quarantine measures on chemical compositions of $PM_{2.5}$ during the COVID-19 epidemic in Shanghai, China. *The Science of the Total Environment*, *743*, 140758. https://doi.org/10.1016/j.scitotenv.2020.140758

Chen, Q., Heald, C. L., Jimenez, J. L., Canagaratna, M. R., Zhang, Q., He, L. Y., et al. (2015). Elemental composition of organic aerosol: The gap between ambient and laboratory measurements. *Geophysical Research Letters*, *42*(10), 4182–4189. https://doi.org/10.1002/2015GL063693

Colberg, C. A., Luo, B. P., Wernli, H., Koop, T., & Peter, T. (2003). A novel model to predict the physical state of atmospheric $H_2SO_4/NH_3/H_2O$ aerosol particles. *Atmospheric Chemistry and Physics*, *3*(4), 909–924. https://doi.org/10.5194/acp-3-909-2003

Crippa, M., El Haddad, I., Slowik, J. G., DeCarlo, P. F., Mohr, C., Heringa, M. F., et al. (2013). Identification of marine and continental aerosol sources in Paris using high resolution aerosol mass spectrometry. *Journal of Geophysical Research: Atmospheres*, *118*(4), 1950–1963. https://doi.org/10.1002/jgrd.50151

DeCarlo, P. F., Dunlea, E. J., Kimmel, J. R., Aiken, A. C., Sueper, D., Crounse, J., et al. (2008). Fast airborne aerosol size and chemistry measurements above Mexico City and Central Mexico during the MILAGRO campaign. *Atmospheric Chemistry and Physics*, *8*, 4027–4048. https://doi.org/10.5194/acp-8-4027-2008

DeCarlo, P. F., Ulbrich, I. M., Crounse, J., de Foy, B., Dunlea, E. J., Aiken, A. C., et al. (2010). Investigation of the sources and processing of organic aerosol over the Central Mexican Plateau from aircraft measurements during MILAGRO. *Atmospheric Chemistry and Physics*, *10*(12), 5257–5280. https://doi.org/10.5194/acp-10-5257-2010

De Gouw, J., & Jimenez, J. L. (2009). Organic aerosols in the Earth's atmosphere. *Environmental Science & Technology*, *43*, 7614–7618. https://doi.org/10.1021/es9006004

de Gouw, J. A., Gilman, J. B., Kim, S.-W., Lerner, B. M., Isaacman-VanWertz, G., McDonald, B. C., et al. (2017). Chemistry of volatile organic compounds in the Los Angeles basin: Nighttime removal of alkenes and determination of emission ratios. *Journal of Geophysical Research: Atmospheres*, *122*(21), 11843–11861. https://doi.org/10.1002/2017jd027459

de Gouw, J. A., Middlebrook, A. M., Warneke, C., Goldan, P. D., Kuster, W. C., Roberts, J. M., et al. (2005). Budget of organic carbon in a polluted atmosphere: Results from the New England Air Quality Study in 2002. *Journal of Geophysical Research*, *110*(D16). https://doi.org/10.1029/2004JD005623

de Gouw, J. A., Warneke, C., Stohl, A., Holloway, J., & Fehsenfeld, F. (2005). *Emissions and photochemistry of oxygenated VOCs in the outflow from urban centers in the Northeastern U.S*. AGU Fall Meeting Abstracts.

Docherty, K. S., Aiken, A. C., Huffman, J. A., Ulbrich, I. M., DeCarlo, P. F., Sueper, D., et al. (2011). The 2005 Study of Organic Aerosols at Riverside (SOAR-1): Instrumental intercomparisons and fine particle composition. *Atmospheric Chemistry and Physics*, *11*(23), 12387–12420. https://doi.org/10.5194/acp-11-12387-2011

Dockery, D. W. (2009). Health effects of particulate air pollution. *Annals of Epidemiology*, *19*(4), 257–263. https://doi.org/10.1016/j.annepidem.2009.01.018

Drinovec, L., Močnik, G., Zotter, P., Prévôt, A. S. H., Ruckstuhl, C., Coz, E., et al. (2015). The "dual-spot" Aethalometer: An improved measurement of aerosol black carbon with real-time loading compensation. *Atmospheric Measurement Techniques*, *8*(5), 1965–1979. https://doi.org/10.5194/amt-8-1965-2015

Dzepina, K., Cappa, C. D., Volkamer, R. M., Madronich, S., DeCarlo, P. F., Zaveri, R. A., & Jimenez, J. L. (2011). Modeling the multiday evolution and aging of secondary organic aerosol during MILAGRO 2006. *Environmental Science & Technology*, *45*(8), 3496–3503. https://doi.org/10.1021/es103186f

Dzepina, K., Volkamer, R. M., Madronich, S., Tulet, P., Ulbrich, I. M., Zhang, Q., et al. (2009). Evaluation of recently-proposed secondary organic aerosol models for a case study in Mexico City. *Atmospheric Chemistry and Physics*, *9*(15), 5681–5709. https://doi.org/10.5194/acp-9-5681-2009

Elser, M., Huang, R.-J., Wolf, R., Slowik, J. G., Wang, Q., Canonaco, F., et al. (2016). New insights into $PM_{2.5}$ chemical composition and sources in two major cities in China during extreme haze events using aerosol mass spectrometry. *Atmospheric Chemistry and Physics*, *16*(5), 3207–3225. https://doi.org/10.5194/acp-16-3207-2016

Fang, X., Fan, Q., Liao, Z., Xie, J., Xu, X., & Fan, S. (2019). Spatial-temporal characteristics of the air quality in the Guangdong-Hong Kong-Macau Greater Bay Area of China during 2015–2017. *Atmospheric Environment*, *210*, 14–34. https://doi.org/10.1016/j.atmosenv.2019.04.037

Farmer, D. K., Matsunaga, A., Docherty, K. S., Surratt, J. D., Seinfeld, J. H., Ziemann, P. J., & Jimenez, J. L. (2010). Response of an aerosol mass spectrometer to organonitrates and organosulfates and implications for atmospheric chemistry. *Proceedings of the National Academy of Sciences of the United States of America*, *107*(15), 6670–6675. https://doi.org/10.1073/pnas.0912340107

Fountoukis, C., & Nenes, A. (2007). ISOTROPIC II: A computationally efficient thermodynamic equilibrium model for K^+–Ca^{2+}–Mg^{2+}–NH^{4+}–Na^+–SO_4^{2-}–NO^{3-}–Cl^-–H_2O aerosols. *Atmospheric Chemistry and Physics*. https://doi.org/10.5194/acpd-7-1893-2007

Fry, J. L., Draper, D. C., Zarzana, K. J., Campuzano-Jost, P., Day, D. A., Jimenez, J. L., et al. (2013). Observations of gas- and aerosol-phase organic nitrates at BEACHON-RoMBAS 2011. *Atmospheric Chemistry and Physics*, *13*(17), 8585–8605. https://doi.org/10.5194/acp-13-8585-2013

Fu, X., Wang, T., Gao, J., Wang, P., Liu, Y., Wang, S., et al. (2020). Persistent heavy winter nitrate pollution driven by increased photochemical oxidants in Northern China. *Environmental Science & Technology*, *54*(7), 3881–3889. https://doi.org/10.1021/acs.est.9b07248

Ge, X., Setyan, A., Sun, Y., & Zhang, Q. (2012). Primary and secondary organic aerosols in Fresno, California during wintertime: Results from high resolution aerosol mass spectrometry. *Journal of Geophysical Research*, *117*(D19). https://doi.org/10.1029/2012jd018026

Ge, X., Zhang, Q., Sun, Y., Ruehl, C., & Setyan, A. (2012). Effect of aqueous-phase processing on aerosol chemistry and size distributions in Fresno, California, during wintertime. *Environmental Chemistry*, *9*, 221–235. https://doi.org/10.1071/EN11168

George, I., & Abbatt, J. (2010). Heterogeneous oxidation of atmospheric aerosol particles by gas-phase radicals. *Nature Chemistry*, *2*, 713–722. https://doi.org/10.1038/nchem.806

Gong, Z., Lan, Z., Xue, L., Zeng, L., He, L., & Huang, X. (2012). Characterization of submicron aerosols in the urban outflow of the central Pearl River Delta region of China. *Frontiers of Environmental Science & Engineering*, *6*(5), 725–733. https://doi.org/10.1007/s11783-012-0441-8

Griffith, S. M., Huang, X. H. H., Louie, P. K. K., & Yu, J. Z. (2015). Characterizing the thermodynamic and chemical composition factors controlling $PM_{2.5}$ nitrate: Insights gained from two years of online measurements in Hong Kong. *Atmospheric Environment*, *122*, 864–875. https://doi.org/10.1016/j.atmosenv.2015.02.009

Guo, H., Sullivan, A. P., Campuzano-Jost, P., Schroder, J. C., Lopez-Hilfiker, F. D., Dibb, J. E., et al. (2016). Fine particle pH and the partitioning of nitric acid during winter in the northeastern United States. *Journal of Geophysical Research: Atmospheres*, *121*(17), 10355–10376. https://doi.org/10.1002/2016jd025311

Guo, H., Xu, L., Bougiatioti, A., Cerully, K. M., Capps, S. L., Hite, J. R., et al. (2015). Fine-particle water and pH in the southeastern United States. *Atmospheric Chemistry and Physics*, *15*(9), 5211–5228. https://doi.org/10.5194/acp-15-5211-2015

Guo, H., Zou, S. C., Tsai, W. Y., Chan, L. Y., & Blake, D. R. (2011). Emission characteristics of nonmethane hydrocarbons from private cars and taxis at different driving speeds in Hong Kong. *Atmospheric Environment*, *45*(16), 2711–2721. https://doi.org/10.1016/j.atmosenv.2011.02.053

Guo, J., Zhou, S., Cai, M., Zhao, J., Song, W., Zhao, W., et al. (2020). *Characterization of submicron particles by time-of-flight aerosol chemical speciation monitor (ToF-ACSM) during wintertime: Aerosol composition, sources and chemical processes in Guangzhou, China*. https://doi.org/10.5194/acp-2019-1080

Hallquist, M., Wenger, J. C., Baltensperger, U., Rudich, Y., Simpson, D., Claeys, M., et al. (2009). The formation, properties and impact of secondary organic aerosol: Current and emerging issues. *Atmospheric Chemistry and Physics*, *9*(14), 5155–5236. https://doi.org/10.5194/acp-9-5155-2009

Hayes, P. L., Ortega, A. M., Cubison, M. J., Froyd, K. D., Zhao, Y., Cliff, S. S., et al. (2013). Organic aerosol composition and sources in Pasadena, California, during the 2010 CalNex campaign. *Journal of Geophysical Research: Atmospheres*, *118*(16), 9233–9257. https://doi.org/10.1002/jgrd.50530

He, L.-Y., Huang, X.-F., Xue, L., Hu, M., Lin, Y., Zheng, J., et al. (2011). Submicron aerosol analysis and organic source apportionment in an urban atmosphere in Pearl River Delta of China using high-resolution aerosol mass spectrometry. *Journal of Geophysical Research*, *116*(D12). https://doi.org/10.1029/2010jd014566

Heald, C., Kroll, J., Jimenez, J., Docherty, K., DeCarlo, P., Aiken, A., et al. (2010). A simplified description of the evolution of organic aerosol composition in the atmosphere. *Geophysical Research Letters*, *37*. https://doi.org/10.1029/2010GL042737

Hodzic, A., & Jimenez, J. L. (2011). Modeling anthropogenically controlled secondary organic aerosols in a megacity: A simplified framework for global and climate models. *Geoscientific Model Development*, *4*(4), 901–917. https://doi.org/10.5194/gmd-4-901-2011

Hong-li, W., Sheng-ao, J., Sheng-rong, L., Qing-yao, H., Li, L., Shi-kang, T., et al. (2017). Volatile organic compounds (VOCs) source profiles of on-road vehicle emissions in China. *The Science of the Total Environment*, *607–608*, 253–261. https://doi.org/10.1016/j.scitotenv.2017.07.001

Hou, X., Chan, C. K., Dong, G. H., & Yim, S. H. L. (2019). Impacts of transboundary air pollution and local emissions on $PM_{2.5}$ pollution in the Pearl River Delta region of China and the public health, and the policy implications. *Environmental Research Letters*, *14*(3), 034005. https://doi.org/10.1088/1748-9326/aaf493

Hu, W., Campuzano-Jost, P., Day, D. A., Croteau, P., Canagaratna, M. R., Jayne, J. T., et al. (2017). Evaluation of the new capture vaporizer for aerosol mass spectrometers (AMS) through field studies of inorganic species. *Aerosol Science and Technology*, *51*(6), 735–754. https://doi.org/10.1080/02786826.2017.1296104

Hu, W., Campuzano-Jost, P., Day, D. A., Nault, B. A., Park, T., Lee, T., et al. (2020). Ambient quantification and size distributions for organic aerosol in aerosol mass spectrometers with the new capture vaporizer. *ACS Earth and Space Chemistry*, *4*(5), 676–689. https://doi.org/10.1021/acsearthspacechem.9b00310

Hu, W., Hu, M., Hu, W., Jimenez, J. L., Yuan, B., Chen, W., et al. (2016). Chemical composition, sources, and aging process of submicron aerosols in Beijing: Contrast between summer and winter. *Journal of Geophysical Research: Atmospheres*, *121*(4), 1955–1977. https://doi.org/10.1002/2015jd024020

Hu, W., Hu, M., Hu, W.-W., Niu, H., Zheng, J., Wu, Y., et al. (2016). Characterization of submicron aerosols influenced by biomass burning at a site in the Sichuan Basin, southwestern China. *Atmospheric Chemistry and Physics*, *16*(20), 13213–13230. https://doi.org/10.5194/acp-16-13213-2016

Hu, W., Hu, M., Hu, W. W., Zheng, J., Chen, C., Wu, Y., & Guo, S. (2017). Seasonal variations in high time-resolved chemical compositions, sources, and evolution of atmospheric submicron aerosols in the megacity Beijing. *Atmospheric Chemistry and Physics*, *17*(16), 9979–10000. https://doi.org/10.5194/acp-17-9979-2017

Hu, W., Palm, B. B., Day, D. A., Campuzano-Jost, P., Krechmer, J. E., Peng, Z., et al. (2016). Volatility and lifetime against OH heterogeneous reaction of ambient isoprene-epoxydiols-derived secondary organic aerosol (IEPOX-SOA). *Atmospheric Chemistry and Physics*, *16*, 11563–11580. https://doi.org/10.5194/acp-16-11563-2016

Hu, W. W., Hu, M., Yuan, B., Jimenez, J. L., Tang, Q., Peng, J. F., et al. (2013). Insights on organic aerosol aging and the influence of coal combustion at a regional receptor site of central eastern China. *Atmospheric Chemistry and Physics*, *13*(19), 10095–10112. https://doi.org/10.5194/acp-13-10095-2013

Huang, X. F., He, L.-Y., Hu, M., Canagaratna, M. R., Kroll, J. H., Ng, N. L., et al. (2011). Characterization of submicron aerosols at a rural site in Pearl River Delta of China using an Aerodyne High-Resolution Aerosol Mass Spectrometer. *Atmospheric Chemistry and Physics*, *11*(5), 1865–1877. https://doi.org/10.5194/acp-11-1865-2011

Huang, X. F., He, L.-Y., Hu, M., Canagaratna, M. R., Sun, Y., Zhang, Q., et al. (2010). Highly time-resolved chemical characterization of atmospheric submicron particles during 2008 Beijing Olympic Games using an Aerodyne High-Resolution Aerosol Mass Spectrometer. *Atmospheric Chemistry and Physics*, *10*(18), 8933–8945. https://doi.org/10.5194/acp-10-8933-2010

IPCC. (2018). *Expert meeting of the intergovernmental panel on climate change on assessing climate information for regions, IPCC working group I technical support unit* (p. 50). Université Paris Saclay, Saint Aubin, France.

Isaacman, G., Chan, A. W., Nah, T., Worton, D. R., Ruehl, C. R., Wilson, K. R., & Goldstein, A. H. (2012). Heterogeneous OH oxidation of motor oil particles causes selective depletion of branched and less cyclic hydrocarbons. *Environmental Science & Technology*, *46*(19), 10632–10640. https://doi.org/10.1021/es302768a

Jayne, J. T., Leard, D. C., Zhang, X., Davidovits, P., Smith, K. A., Kolb, C. E., & Worsnop, D. R. (2000). Development of an Aerosol Mass Spectrometer for size and composition analysis of submicron particles. *Aerosol Science and Technology*, *33*(1–2), 49–70. https://doi.org/10.1080/027868200410840

Jimenez, J. L., Canagaratna, M. R., Donahue, N. M., Prevot, A. S. H., Zhang, Q., Kroll, J. H., et al. (2009). Evolution of organic aerosols in the atmosphere. *Science*, *326*(5959), 1525–1529. https://doi.org/10.1126/science.1180353

Jimenez, J. L., Canagaratna, M. R., Drewnick, F., Allan, J. D., Alfarra, M. R., Middlebrook, A. M., et al. (2016). Comment on "The effects of molecular weight and thermal decomposition on the sensitivity of a thermal desorption aerosol mass spectrometer. *Aerosol Science & Technology*, *50*(9). https://doi.org/10.1080/02786826.2016.1205728

Kang, E., Root, M. J., Toohey, D. W., & Brune, W. H. (2007). Introducing the concept of Potential Aerosol Mass (PAM). *Atmospheric Chemistry and Physics*, *7*(22), 5727–5744. https://doi.org/10.5194/acp-7-5727-2007

Katz, E. F., Guo, H., Campuzano-Jost, P., Day, D. A., Brown, W. L., Boedicker, E., et al. (2021). Quantification of cooking organic aerosol in the indoor environment using aerodyne aerosol mass spectrometers. *Aerosol Science and Technology*, 1–16. https://doi.org/10.1080/02786826.2021.1931013

Kessler, S. H., Nah, T., Daumit, K. E., Smith, J. D., Leone, S. R., Kolb, C. E., et al. (2012). OH-initiated heterogeneous aging of highly oxidized organic aerosol. *The Journal of Physical Chemistry A*, *116*(24), 6358–6365. https://doi.org/10.1021/jp212131m

Kessler, S. H., Smith, J. D., Che, D. L., Worsnop, D. R., Wilson, K. R., & Kroll, J. H. (2010). Chemical sinks of organic aerosol: Kinetics and products of the heterogeneous oxidation of Erythritol and Levoglucosan. *Environmental Science & Technology*, *44*(18), 7005–7010. https://doi.org/10.1021/es101465m

Kim, H., Zhang, Q., Bae, G.-N., Kim, J. Y., & Lee, S. B. (2017). Sources and atmospheric processing of winter aerosols in Seoul, Korea: Insights from real-time measurements using a high-resolution aerosol mass spectrometer. *Atmospheric Chemistry and Physics*, *17*(3), 2009–2033. https://doi.org/10.5194/acp-17-2009-2017

Kroll, J. H., Donahue, N. M., Jimenez, J. L., Kessler, S. H., Canagaratna, M. R., Wilson, K. R., et al. (2011). Carbon oxidation state as a metric for describing the chemistry of atmospheric organic aerosol. *Nature Chemistry*, *3*(2), 133–139. https://doi.org/10.1038/NCHEM.948

Kroll, J. H., Lim, C. Y., Kessler, S. H., & Wilson, K. R. (2015). Heterogeneous oxidation of atmospheric organic aerosol: Kinetics of changes to the amount and oxidation state of particle-phase organic carbon. *The Journal of Physical Chemistry A*, *119*(44), 10767–10783. https://doi.org/10.1021/acs.jpca.5b06946

Kuwata, M., Zorn, S. R., & Martin, S. T. (2011). Using elemental ratios to predict the density of organic material composed of carbon, hydrogen, and oxygen. *Environmental Science & Technology*, *46*(2), 787–794. https://doi.org/10.1021/es202525q

Lambe, A. T., Ahern, A. T., Williams, L. R., Slowik, J. G., Wong, J. P. S., Abbatt, J. P. D., et al. (2011). Characterization of aerosol photooxidation flow reactors: Heterogeneous oxidation, secondary organic aerosol formation and cloud condensation nuclei activity measurements. *Atmospheric Measurement Techniques*, *4*(3), 445–461. https://doi.org/10.5194/amt-4-445-2011

Lanz, V. A., Alfarra, M. R., Baltensperger, U., Buchmann, B., Hueglin, C., & Prevot, A. S. H. (2007). Source apportionment of submicron organic aerosols at an urban site by factor analytical modelling of aerosol mass spectra. *Atmospheric Chemistry and Physics*, *7*(6), 1503–1522. https://doi.org/10.5194/acp-7-1503-2007

Li, H., Zhang, Q., Zheng, B., Chen, C., Wu, N., Guo, H., et al. (2018). Nitrate-driven urban haze pollution during summertime over the North China Plain. *Atmospheric Chemistry and Physics*, *18*(8), 5293–5306. https://doi.org/10.5194/acp-18-5293-2018

Li, R., Palm, B. B., Ortega, A. M., Hlywiak, J., Hu, W., Peng, Z., et al. (2015). Modeling the radical chemistry in an oxidation flow reactor: Radical formation and recycling, sensitivities, and the OH exposure estimation equation. *The Journal of Physical Chemistry A*, *119*(19), 4418–4432. https://doi.org/10.1021/jp509534k

Li, W., Liu, X., Zhang, Y., Sun, K., Wu, Y., Xue, R., et al. (2018). Characteristics and formation mechanism of regional haze episodes in the Pearl River Delta of China. *Journal of Environmental Sciences*, *63*, 236–249. https://doi.org/10.1016/j.jes.2017.03.018

Li, Y. J., Lee, B. P., Su, L., Fung, J. C. H., & Chan, C. K. (2015). Seasonal characteristics of fine particulate matter (PM) based on high-resolution time-of-flight aerosol mass spectrometric (HR-ToF-AMS) measurements at the HKUST Supersite in Hong Kong. *Atmospheric Chemistry and Physics*, *15*, 37–53. https://doi.org/10.5194/acp-15-37-2015

Li, Y. J., Liu, P., Gong, Z., Wang, Y., Bateman, A. P., Bergoend, C., et al. (2015). Chemical reactivity and liquid/nonliquid states of secondary organic material. *Environmental Science & Technology*, *49*(22), 13264–13274. https://doi.org/10.1021/acs.est.5b03392

Li, Y. J., Sun, Y., Zhang, Q., Li, X., Li, M., Zhou, Z., & Chan, C. K. (2017). Real-time chemical characterization of atmospheric particulate matter in China: A review. *Atmospheric Environment*, *158*, 270–304. https://doi.org/10.1016/j.atmosenv.2017.02.027

Lin, C., Li, Y., Lau, A. K. H., Li, C., & Fung, J. C. H. (2018). 15-Year $PM_{2.5}$ trends in the Pearl River Delta Region and Hong Kong from satellite observation. *Aerosol and Air Quality Research*, *18*(9), 2355–2362. https://doi.org/10.4209/aaqr.2017.11.0437

Lin, Y. C., Zhang, Y. L., Fan, M. Y., & Bao, M. (2020). Heterogeneous formation of particulate nitrate under ammonium-rich regimes during the high-$PM_{2.5}$ events in Nanjing, China. *Atmospheric Chemistry and Physics*, *20*(6), 3999–4011. https://doi.org/10.5194/acp-20-3999-2020

Liu, T., Zhou, L., Liu, Q., Lee, B. P., Yao, D., Lu, H., et al. (2019). Secondary organic aerosol formation from urban roadside air in Hong Kong. *Environmental Science & Technology*, *53*(6), 3001–3009. https://doi.org/10.1021/acs.est.8b06587

Liu, X., Sun, K., Qu, Y., Hu, M., Sun, Y., Zhang, F., & Zhang, Y. (2015). Secondary formation of sulfate and nitrate during a haze episode in megacity Beijing, China. *Aerosol and Air Quality Research*, *15*(6), 2246–2257. https://doi.org/10.4209/aaqr.2014.12.0321

Liu, Y., Wu, Z., Huang, X., Shen, H., Bai, Y., Qiao, K., et al. (2019). Aerosol phase state and its link to chemical composition and liquid water content in a subtropical coastal megacity. *Environmental Science & Technology*, *53*(9), 5027–5033. https://doi.org/10.1021/acs.est.9b01196

Lu, X., Chen, Y., Huang, Y., Lin, C., Li, Z., Fung, J. C. H., & Lau, A. K. H. (2019). Differences in concentration and source apportionment of PM2.5 between 2006 and 2015 over the PRD region in southern China. *The Science of the Total Environment*, *673*, 708–718. https://doi.org/10.1016/j.scitotenv.2019.03.452

Lu, X., Zhang, S., Xing, J., Wang, Y., Chen, W., Ding, D., et al. (2020). Progress of Air pollution control in China and its challenges and opportunities in the ecological civilization era. *Engineering*, *6*(12), 1423–1431. https://doi.org/10.1016/j.eng.2020.03.014

Luo, L., Kao, S., Wu, Y., Zhang, X., Lin, H., Zhang, R., & Xiao, H. (2020). Stable oxygen isotope constraints on nitrate formation in Beijing in springtime. *Environmental Pollution*, *263*(Pt B), 114515. https://doi.org/10.1016/j.envpol.2020.114515

Ma, Z., Liu, R., Liu, Y., & Bi, J. (2019). Effects of air pollution control policies on PM2.5 pollution improvement in China from 2005 to 2017: A satellite-based perspective. *Atmospheric Chemistry and Physics*, *19*(10), 6861–6877. https://doi.org/10.5194/acp-19-6861-2019

Mao, J., Ren, X., Brune, W. H., Olson, J. R., Crawford, J. H., Fried, A., et al. (2009). Airborne measurement of OH reactivity during INTEX-B. *Atmospheric Chemistry and Physics*, *9*(1), 163–173. https://doi.org/10.5194/acp-9-163-2009

Matthew, B. M., Middlebrook, A. M., & Onasch, T. B. (2008). Collection efficiencies in an aerodyne aerosol mass spectrometer as a function of particle phase for laboratory generated aerosols. *Aerosol Science and Technology*, *42*(11), 884–898. https://doi.org/10.1080/02786820802356797

McNeill, V. F., Yatavelli, R. L. N., Thornton, J. A., Stipe, C. B., & Landgrebe, O. (2008). Heterogeneous OH oxidation of palmitic acid in single component and internally mixed aerosol particles: Vaporization and the role of particle phase. *Atmospheric Chemistry and Physics*, *8*(17), 5465–5476. https://doi.org/10.5194/acp-8-5465-2008

Middlebrook, A. M., Bahreini, R., Jimenez, J. L., & Canagaratna, M. R. (2012). Evaluation of composition-dependent collection efficiencies for the aerodyne aerosol mass spectrometer using field data. *Aerosol Science and Technology*, *46*(3), 258–271. https://doi.org/10.1080/02786826.2011.620041

Molina, M. J., & Molina, L. T. (2004). Megacities and atmospheric pollution. *Journal of the Air & Waste Management Association*, *54*(6), 644–680. https://doi.org/10.1080/10473289.2004.10470936

Nault, B. A., Campuzano-Jost, P., Day, D. A., Schroder, J. C., Anderson, B., Beyersdorf, A. J., et al. (2018). Secondary organic aerosol production from local emissions dominates the organic aerosol budget over Seoul, South Korea, during KORUS-AQ. *Atmospheric Chemistry and Physics*, *18*(24), 17769–17800. https://doi.org/10.5194/acp-18-17769-2018

Ng, N. L., Canagaratna, M. R., Jimenez, J. L., Chhabra, P. S., Seinfeld, J. H., & Worsnop, D. R. (2011). Changes in organic aerosol composition with aging inferred from aerosol mass spectra. *Atmospheric Chemistry and Physics*, *11*(13), 6465–6474. https://doi.org/10.5194/acp-11-6465-2011

Ng, N. L., Canagaratna, M. R., Jimenez, J. L., Zhang, Q., Ulbrich, I. M., & Worsnop, D. R. (2011). Real-time methods for estimating organic component mass concentrations from aerosol mass spectrometer data. *Environmental Science & Technology*, *45*(3), 910–916. https://doi.org/10.1021/es102951k

Ng, N. L., Canagaratna, M. R., Zhang, Q., Jimenez, J. L., Tian, J., Ulbrich, I. M., et al. (2010). Organic aerosol components observed in Northern Hemispheric datasets from Aerosol Mass Spectrometry. *Atmospheric Chemistry and Physics*, *10*(10), 4625–4641. https://doi.org/10.5194/acp-10-4625-2010

Ortega, A. M., Hayes, P. L., Peng, Z., Palm, B. B., Hu, W., Day, D. A., et al. (2016). Real-time measurements of secondary organic aerosol formation and aging from ambient air in an oxidation flow reactor in the Los Angeles area. *Atmospheric Chemistry and Physics*, *16*(11), 7411–7433. https://doi.org/10.5194/acp-16-7411-2016

Ovadnevaite, J., Ceburnis, D., & Kvietkus, K. (2007). Chemical composition and size distribution of fine aerosol particles on the east coast of the Baltic Sea. *Lithuanian Journal of Physics*, *47*. https://doi.org/10.1007/978-1-4020-6475-3_157

Paatero, P. (1999). The multilinear engine—A table-driven, least squares program for solving multilinear problems, including the n-way parallel factor analysis model. *Journal of Computational & Graphical Statistics*, *8*(4), 854–888. https://doi.org/10.1080/10618600.1999.10474853

Paatero, P., & Tapper, U. (1994). Positive matrix factorization: A non-negative factor model with optimal utilization of error estimates of data value". *Environmetrics*, *5*, 111–126. https://doi.org/10.1002/env.3170050203

Pajunoja, A., Hu, W., Leong, Y. J., Taylor, N. F., Miettinen, P., Palm, B. B., et al. (2016). Phase state of ambient aerosol linked with water uptake and chemical aging in the southeastern US. *Atmospheric Chemistry and Physics*, *16*(17), 11163–11176. https://doi.org/10.5194/acp-16-11163-2016

Palm, B. B., de Sá, S. S., Day, D. A., Campuzano-Jost, P., Hu, W., Seco, R., et al. (2018). Secondary organic aerosol formation from ambient air in an oxidation flow reactor in central Amazonia. *Atmospheric Chemistry and Physics*, *18*(1), 467–493. https://doi.org/10.5194/acp-18-467-2018

Peng, Z., Day, D. A., Stark, H., Li, R., Lee-Taylor, J., Palm, B. B., et al. (2015). HOx radical chemistry in oxidation flow reactors with low-pressure mercury lamps systematically examined by modeling. *Atmospheric Measurement Techniques*, *8*(11), 4863–4890. https://doi.org/10.5194/amt-8-4863-2015

Pieber, S. M., El Haddad, I., Slowik, J. G., Canagaratna, M. R., Jayne, J. T., Platt, S. M., et al. (2016). Inorganic salt interference on CO2(+) in aerodyne AMS and ACSM organic aerosol composition studies. *Environmental Science & Technology*, *50*(19), 10494–10503. https://doi.org/10.1021/acs.est.6b01035

Pope, C. A., 3rd, Ezzati, M., & Dockery, D. W. (2009). Fine-particulate air pollution and life expectancy in the United States. *New England Journal of Medicine*, *360*(4), 376–386. https://doi.org/10.1056/NEJMsa0805646

Poschl, U. (2005). Atmospheric aerosols: Composition, transformation, climate and health effects. *Angewandte Chemie International Edition in English*, *44*(46), 7520–7540. https://doi.org/10.1002/anie.200501122

Qin, Y., Tan, H., Li, Y., Schurman, M., Li, F., Canonaco, F., et al. (2017). Impacts of traffic emissions on atmospheric particulate nitrate and organics at a downwind site on the periphery of Guangzhou, China. *Atmospheric Chemistry and Physics*, *17*, 10245–10258. https://doi.org/10.5194/acp-17-10245-2017

Qiu, X., Ying, Q., Wang, S., Duan, L., Zhao, J., Xing, J., et al. (2019). Modeling the impact of heterogeneous reactions of chlorine on summertime nitrate formation in Beijing, China. *Atmospheric Chemistry and Physics*, *19*(10), 6737–6747. https://doi.org/10.5194/acp-19-6737-2019

Reyes-Villegas, E., Bannan, T., Le Breton, M., Mehra, A., Priestley, M., Percival, C., et al. (2018). Online chemical characterization of food-cooking organic aerosols: implications for source apportionment. *Environmental Science & Technology*, *52*(9), 5308–5318. https://doi.org/10.1021/acs.est.7b06278

Schroder, J. C., Campuzano-Jost, P., Day, D. A., Shah, V., Larson, K., Sommers, J. M., et al. (2018). Sources and secondary production of organic aerosols in the Northeastern United States during WINTER. *Journal of Geophysical Research: Atmospheres*, *123*, 7771–7796. https://doi.org/10.1029/2018jd028475

Seinfeld, J. H., & Pandis, S. N. (2006). *Atmospheric chemistry and Physics: From air pollution to climate change*, ISBN-13: 978-970-471-72018-72018, 72006 pp.

Sengupta, D., Samburova, V., Bhattarai, C., Watts, A. C., Moosmüller, H., & Khlystov, A. Y. (2020). Polar semivolatile organic compounds in biomass-burning emissions and their chemical transformations during aging in an oxidation flow reactor. *Atmospheric Chemistry and Physics*, *20*(13), 8227–8250. https://doi.org/10.5194/acp-20-8227-2020

Slade, J. H., & Knopf, D. A. (2014). Multiphase OH oxidation kinetics of organic aerosol: The role of particle phase state and relative humidity. *Geophysical Research Letters*, *41*(14), 5297–5306. https://doi.org/10.1002/2014gl060582

Smith, J. D., Kroll, J. H., Cappa, C. D., Che, D. L., Liu, C. L., Ahmed, M., et al. (2009). The heterogeneous reaction of hydroxyl radicals with sub-micron squalane particles: A model system for understanding the oxidative aging of ambient aerosols. *Atmospheric Chemistry and Physics*, *9*(9), 3209–3222. https://doi.org/10.5194/acp-9-3209-2009

Spracklen, D. V., Jimenez, J. L., Carslaw, K. S., Worsnop, D. R., Evans, M. J., Mann, G. W., et al. (2011). Aerosol mass spectrometer constraint on the global secondary organic aerosol budget. *Atmospheric Chemistry and Physics*, *11*(23), 12109–12136. https://doi.org/10.5194/acp-11-12109-2011

Sun, J., Zhang, Q., Canagaratna, M. R., Zhang, Y., Ng, N. L., Sun, Y., et al. (2010). Highly time- and size-resolved characterization of submicron aerosol particles in Beijing using an Aerodyne Aerosol Mass Spectrometer. *Atmospheric Environment*, *44*(1), 131–140. https://doi.org/10.1016/j.atmosenv.2009.03.020

Sun, Y., Du, W., Fu, P., Wang, Q., Li, J., Ge, X., et al. (2016). Primary and secondary aerosols in Beijing in winter: Sources, variations and processes. *Atmospheric Chemistry and Physics*, *16*(13), 8309–8329. https://doi.org/10.5194/acp-16-8309-2016

Sun, Y. L., Wang, Z. F., Fu, P. Q., Yang, T., Jiang, Q., Dong, H. B., et al. (2013), Aerosol composition, sources and processes during wintertime in Beijing, China. *Atmospheric Chemistry and Physics*, *13*(9), 4577–4592. https://doi.org/10.5194/acp-13-4577-2013

Sun, Y. L., Zhang, Q., Schwab, J. J., Demerjian, K. L., Chen, W.-N., Bae, M.-S., et al. (2011). Characterization of the sources and processes of organic and inorganic aerosols in New York city with a high-resolution time-of-flight aerosol mass apectrometer. *Atmospheric Chemistry and Physics*, *11*(4), 1581–1602. https://doi.org/10.5194/acp-11-1581-2011

Takhar, M., Stroud, C. A., & Chan, A. W. H. (2019). Volatility distribution and evaporation rates of organic aerosol from cooking oils and their evolution upon heterogeneous oxidation. *ACS Earth and Space Chemistry*, *3*, 1717–1728. https://doi.org/10.1021/acsearthspacechem.9b00110

Thornton, J., Braban, C., & Abbatt, J. (2003). N2O5 Hydrolysis on sub-micron organic aerosols: The effect of relative humidity, particle phase, and particle size. *Physical Chemistry Chemical Physics*, *5*, 4593. https://doi.org/10.1039/B307498F

Ulbrich, I. M., Canagaratna, M. R., Zhang, Q., Worsnop, D. R., & Jimenez, J. L. (2009). Interpretation of organic components from Positive Matrix Factorization of aerosol mass spectrometric data. *Atmospheric Chemistry and Physics*, *9*(9), 2891–2918. https://doi.org/10.5194/acp-9-2891-2009

Wang, C., Yuan, B., Wu, C., Wang, S., Qi, J., Wang, B., et al. (2020). Measurements of higher alkanes using NO+ chemical ionization in PTR-ToF-MS: Important contributions of higher alkanes to secondary organic aerosols in China. *Atmospheric Chemistry and Physics*, *20*(22), 14123–14138. https://doi.org/10.5194/acp-20-14123-2020

Wang, J., Ge, X., Chen, Y., Shen, Y., Zhang, Q., Sun, Y., et al. (2016). Highly time-resolved urban aerosol characteristics during springtime in Yangtze River Delta, China: Insights from soot particle aerosol mass spectrometry. *Atmospheric Chemistry and Physics*, *16*(14), 9109–9127. https://doi.org/10.5194/acp-16-9109-2016

Wang, J., Zhao, B., Wang, S., Yang, F., Xing, J., Morawska, L., et al. (2017). Particulate matter pollution over China and the effects of control policies. *The Science of the Total Environment*, *584–585*, 426–447. https://doi.org/10.1016/j.scitotenv.2017.01.027

Wang, W., Yu, J., Cui, Y., He, J., Xue, P., Cao, W., et al. (2018). Characteristics of fine particulate matter and its sources in an industrialized coastal city, Ningbo, Yangtze River Delta, China. *Atmospheric Research*, *203*, 105–117. https://doi.org/10.1016/j.atmosres.2017.11.033

Wang, Y., Chen, Y., Wu, Z., Shang, D., Bian, Y., Du, Z., et al. (2020). Mutual promotion between aerosol particle liquid water and particulate nitrate enhancement leads to severe nitrate-dominated particulate matter pollution and low visibility. *Atmospheric Chemistry and Physics*, *20*(4), 2161–2175. https://doi.org/10.5194/acp-20-2161-2020

Wang, Y., Wang, Y., Cao, J., Lin, C., Duan, J., Chen, Q., et al. (2018). Primary emissions versus secondary formation of fine particulate matter in the top polluted city, Shijiazhuang North China, *Atmospheric Chemistry and Physics Discussions*, *19*, 1–38. https://doi.org/10.5194/acp-2018-760

Wang, Y. C., Huang, R.-J., Ni, H. Y., Chen, Y., Wang, Q. Y., Li, G. H., et al. (2017). Chemical composition, sources and secondary processes of aerosols in Baoji city of northwest China. *AtmosEnviron*, *158*, 128–137. https://doi.org/10.1016/j.atmosenv.2017.03.026

Wang, Y.-L., Song, W., Yang, W., Sun, X.-C., Tong, Y.-D., Wang, X.-M., et al. (2019). Influences of atmospheric pollution on the contributions of major oxidation pathways to $PM_{2.5}$ nitrate formation in Beijing. *Journal of Geophysical Research: Atmospheres*, *124*(7), 4174–4185. https://doi.org/10.1029/2019JD030284

Wang, Z., Yuan, B., Ye, C., Roberts, J., Wisthaler, A., Lin, Y., et al. (2020). High concentrations of atmospheric isocyanic acid (HNCO) produced from secondary sources in China. *Environmental Science & Technology*, *54*(19), 11818–11826. https://doi.org/10.1021/acs.est.0c02843

Weitkamp, E. A., Lambe, A. T., Donahue, N. M., & Robinson, A. L. (2008). Laboratory measurements of the heterogeneous oxidation of condensed-phase organic molecular makers for motor vehicle exhaust. *Environmental Science & Technology*, *42*(21), 7950–7956. https://doi.org/10.1021/es800745x

WHO. (2006). *WHO air quality guidelines for particulate matter, ozone, nitrogen dioxide and sulfur dioxide: Global update 2005: Summary of risk assessment*.

Wu, C., Wang, C., Wang, S., Wang, W., Yuan, B., Qi, J., et al. (2020). Measurement report: Important contributions of oxygenated compounds to emissions and chemistry of volatile organic compounds in urban air. *Atmospheric Chemistry and Physics*, *20*(23), 14769–14785. https://doi.org/10.5194/acp-20-14769-2020

Wu, Z., Wang, Y., Tan, T., Zhu, Y., Li, M., Shang, D., et al. (2018). Aerosol liquid water driven by anthropogenic inorganic salts: Implying its key role in haze formation over the North China Plain. *Environmental Science and Technology Letters*, *5*(3), 160–166. https://doi.org/10.1021/acs.estlett.8b00021

Xu, J., Zhang, Q., Chen, M., Ge, X., Ren, J., & Qin, D. (2014). Chemical composition, sources, and processes of urban aerosols during summertime in northwest China: Insights from high-resolution aerosol mass spectrometry. *Atmospheric Chemistry and Physics*, *14*(23), 12593–12611. https://doi.org/10.5194/acp-14-12593-2014

Xu, Q., Wang, S., Jiang, J., Bhattarai, N., Li, X., Chang, X., et al. (2019). Nitrate dominates the chemical composition of PM2.5 during haze event in Beijing, China. *The Science of the Total Environment*, *689*, 1293–1303. https://doi.org/10.1016/j.scitotenv.2019.06.294

Xu, W., Lambe, A., Silva, P., Hu, W., Onasch, T., Williams, L., et al. (2018). Laboratory evaluation of species-dependent relative ionization efficiencies in the Aerodyne Aerosol Mass Spectrometer. *Aerosol Science and Technology*, *52*(6), 626–641. https://doi.org/10.1080/02786826.2018.1439570

Xue, J., Griffith, S. M., Yu, X., Lau, A. K. H., & Yu, J. Z. (2014). Effect of nitrate and sulfate relative abundance in $PM_{2.5}$ on liquid water content explored through half-hourly observations of inorganic soluble aerosols at a polluted receptor site. *Atmospheric Environment*, *99*, 24–31. https://doi.org/10.1016/j.atmosenv.2014.09.049

Yan, F., Chen, W., Jia, S., Zhong, B., Yang, L., Mao, J., et al. (2020). Stabilization for the secondary species contribution to $PM_{2.5}$ in the Pearl River Delta (PRD) over the past decade, China: A meta-analysis. *Atmospheric Environment*, *242*, 117817. https://doi.org/10.1016/j.atmosenv.2020.117817

Yatavelli, R. L. N., Mohr, C., Stark, H., Day, D. A., Thompson, S. L., Lopez-Hilfiker, F. D., et al. (2015). Estimating the contribution of organic acids to northern hemispheric continental organic aerosol. *Geophysical Research Letters*, *42*(14), 6084–6090. https://doi.org/10.1002/2015GL064650

Ye, C., Yuan, B., Lin, Y., Wang, Z., Hu, W., Li, T., et al. (2020). Chemical characterization of oxygenated organic compounds in gas-phase and particle-phase using iodide-CIMS with FIGAERO in urban air. *Atmospheric Chemistry and Physics Discussions*, *2020*, 1–62. https://doi.org/10.5194/acp-2020-1187

Yin, J., Cumberland, S. A., Harrison, R. M., Allan, J., Young, D. E., Williams, P. I., & Coe, H. (2015). Receptor modelling of fine particles in southern England using CMB including comparison with AMS-PMF factors. *Atmospheric Chemistry and Physics*, *15*(4), 2139–2158. https://doi.org/10.5194/acp-15-2139-2015

Yue, D. L., Hu, M., Wu, Z. J., Guo, S., Wen, M. T., Nowak, A., et al. (2010). Variation of particle number size distributions and chemical compositions at the urban and downwind regional sites in the Pearl River Delta during summertime pollution episodes. *Atmospheric Chemistry and Physics*, *10*(19), 9431–9439. https://doi.org/10.5194/acp-10-9431-2010

Zhang, J., Liu, Z., Ji, D., Hu, B., Liu, Q., & Wang, Y. (2013). Characterization of submicron aerosols during a serious pollution month in Beijing (2013) using an aerodyne high-resolution aerosol mass spectrometer. *Atmospheric Chemistry and Physics Discussions*, *13*, 19009–19049. https://doi.org/10.5194/acpd-13-19009-2013

Zhang, Q., Jimenez, J. L., Canagaratna, M. R., Allan, J. D., Coe, H., Ulbrich, I., et al. (2007). Ubiquity and dominance of oxygenated species in organic aerosols in anthropogenically-influenced Northern Hemisphere midlatitudes. *Geophysical Research Letters*, *34*(13). https://doi.org/10.1029/2007gl029979

Zhang, Q., Jimenez, J. L., Canagaratna, M. R., Ulbrich, I. M., Ng, N. L., Worsnop, D. R., & Sun, Y. (2011). Understanding atmospheric organic aerosols via factor analysis of aerosol mass spectrometry: A review. *Analytical and Bioanalytical Chemistry*, *401*(10), 3045–3067. https://doi.org/10.1007/s00216-011-5355-y

Zhang, Q., Worsnop, C., & Jimenez, M. R. (2005). Hydrocarbon-like and oxygenated organic aerosols in Pittsburgh: Insights into sources and processes of organic aerosols. *Atmospheric Chemistry and Physics*, *5*. https://doi.org/10.5194/acpd-5-8421-2005

Zhang, Q., Zheng, Y., Tong, D., Shao, M., Wang, S., Zhang, Y., et al. (2019). Drivers of improved $PM_{2.5}$ air quality in China from 2013 to 2017. *Proceedings of the National Academy of Sciences of the U S A*, *116*(49), 24463–24469. https://doi.org/10.1073/pnas.1907956116

Zhang, Q. J., Beekmann, M., Drewnick, F., Freutel, F., Schneider, J., Crippa, M., et al. (2013). Formation of organic aerosol in the Paris region during the MEGAPOLI summer campaign: Evaluation of the volatility-basis-set approach within the CHIMERE model. *Atmospheric Chemistry and Physics*, *13*(11), 5767–5790. https://doi.org/10.5194/acp-13-5767-2013

Zhang, Y., Tang, L., Yu, H., Wang, Z., Sun, Y., Qin, W., et al. (2015). Chemical composition, sources and evolution processes of aerosol at an urban site in Yangtze River Delta, China during wintertime. *Atmospheric Environment*, *123*, 339–349. https://doi.org/10.1016/j.atmosenv.2015.08.017

Zhao, X. J., Zhao, P. S., Xu, J., Meng, W., Pu, W. W., Dong, F., et al. (2013). Analysis of a winter regional haze event and its formation mechanism in the North China Plain. *Atmospheric Chemistry and Physics*, *13*(11), 5685–5696. https://doi.org/10.5194/acp-13-5685-2013

Zhao, X. Y., Hu, Q., Wang, X., Ding, X., He, Q., Zhang, Z., et al. (2015). Composition profiles of organic aerosols from Chinese residential cooking: Case study in urban Guangzhou, south China. *Journal of Atmospheric Chemistry*, *72*(1), 1–18. https://doi.org/10.1007/s10874-015-9298-0

Zheng, G., Su, H., Wang, S., Andreae, M., Pöschl, U., & Cheng, Y. (2020). Multiphase buffer theory explains contrasts in atmospheric aerosol acidity. *Science*, *369*, 1374–1377. https://doi.org/10.1126/science.aba3719

Zhou, S., Davy, P. K., Huang, M., Duan, J., Wang, X., Fan, Q., et al. (2018). High-resolution sampling and analysis of ambient particulate matter in the Pearl River Delta region of southern China: Source apportionment and health risk implications. *Atmospheric Chemistry and Physics*, *18*(3), 2049–2064. https://doi.org/10.5194/acp-18-2049-2018

Zhou, W., Xu, W., Kim, H., Zhang, Q., Fu, P., Worsnop, D. R., & Sun, Y. (2020). A review of aerosol chemistry in Asia: Insights from aerosol mass spectrometer measurements. *Environmental Science: Processes & Impacts*, *22*, 1616–1653. https://doi.org/10.1039/d0em00212g

Zotter, P., Herich, H., Gysel, M., El-Haddad, I., Zhang, Y., Močnik, G., et al. (2017). Evaluation of the absorption Ångström exponents for traffic and wood burning in the Aethalometer-based source apportionment using radiocarbon measurements of ambient aerosol. *Atmospheric Chemistry and Physics*, *17*(6), 4229–4249. https://doi.org/10.5194/acp-17-4229-2017

References From the Supporting Information

Allan, J. D., Williams, P. I., Morgan, W. T., Martin, C. L., Flynn, M. J., Lee, J., et al. (2010). Contributions from transport, solid fuel burning and cooking to primary organic aerosols in two UK cities. *Atmospheric Chemistry and Physics*, *10*(2), 647. https://doi.org/10.5194/acp-10-647-2010

Dall'Osto, M., Ovadnevaite, J., Ceburnis, D., Martin, D., Healy, R. M., O'Connor, I. P., et al. (2013). Characterization of urban aerosol in Cork city (Ireland) using aerosol mass spectrometry. *Atmospheric Chemistry and Physics*, *13*(9), 4997–5015. https://doi.org/10.5194/acp-13-4997-2013

Florou, K., Papanastasiou, D. K., Pikridas, M., Kaltsonoudis, C., Louvaris, E., Gkatzelis, G. I., et al. (2017). The contribution of wood burning and other pollution sources to wintertime organic aerosol levels in two Greek cities. *Atmospheric Chemistry and Physics*, *17*(4), 3145–3163. https://doi.org/10.5194/acp-17-3145-2017

Frohlich, R., Crenn, V., Setyan, A., Belis, C. A., Canonaco, F., Favez, O., et al. (2015). ACTRIS ACSM intercomparison—Part 2: Intercomparison of ME-2 organic source apportionment results from 15 individual, co-located aerosol mass spectrometers. *Atmospheric Measurement Techniques*, *8*(6), 2555–2576. https://doi.org/10.5194/amt-8-2555-2015

Johnson, A. M., Waring, M. S., & DeCarlo, P. F. (2017). Real-time transformation of outdoor aerosol components upon transport indoors measured with aerosol mass spectrometry. *Indoor Air*, *27*(1), 230–240. https://doi.org/10.1111/ina.12299

Lan, Z., Zhang, B., Huang, X., Zhu, Q., Yuan, J., Zeng, L., et al. (2018). Source apportionment of $PM_{2.5}$ light extinction in an urban atmosphere in China. *Journal of Environmental Sciences*, *63*, 277–284. https://doi.org/10.1016/j.jes.2017.07.016

Lee, B. P., Li, Y. J., Yu, J. Z., Louie, P. K. K., & Chan, C. K. (2013). Physical and chemical characterization of ambient aerosol by HR-ToF-AMS at a suburban site in Hong Kong during springtime 2011. *Journal of Geophysical Research: Atmospheres*, *118*(15), 8625–8639. https://doi.org/10.1002/jgrd.50658

Lee, B. P., Li, Y. J., Yu, J. Z., Louie, P. K. K., & Chan, C. K. (2015). Characteristics of submicron particulate matter at the urban roadside in downtown Hong KongOverview of 4 months of continuous high-resolution aerosol mass spectrometer measurements. *Journal of Geophysical Research: Atmospheres*, *120*(14), 7040–7058. https://doi.org/10.1002/2015jd023311

Li, K., Chen, L., White, S. J., Zheng, X., Lv, B., Lin, C., et al. (2018). Chemical characteristics and sources of PM 1 during the 2016 summer in Hangzhou. *Environmental Pollution*, *232*, 42–54. https://doi.org/10.1016/j.envpol.2017.09.016

Liu, Y., Zhu, W., Wang, Y., & Li, T. (2018). Characterization of atmospheric submicron particles at an urban site in Shanghai in autumn using a high-resolution aerosol mass spectrometer. *Acta Scientiae Circumstantiae*, *38*(7), 2746–2756.

Louvaris, E. E., Florou, K., Karnezi, E., Papanastasiou, D. K., Gkatzelis, G. I., & Pandis, S. N. (2017). Volatility of source apportioned wintertime organic aerosol in the city of Athens. *Atmospheric Environment*, *158*, 138–147. https://doi.org/10.1016/j.atmosenv.2017.03.042

Mei, F., Setyan, A., Zhang, Q., & Wang, J. (2013). CCN activity of organic aerosols observed downwind of urban emissions during CARES. *Atmospheric Chemistry and Physics*, *13*(24), 12155–12169. https://doi.org/10.5194/acp-13-12155-2013

Mohr, C., DeCarlo, P. F., Heringa, M. F., Chirico, R., Slowik, J. G., Richter, R., et al. (2012). Identification and quantification of organic aerosol from cooking and other sources in Barcelona using aerosol mass spectrometer data. *Atmospheric Chemistry and Physics*, *12*(4), 1649–1665. https://doi.org/10.5194/acp-12-1649-2012

Paciga, A., Karnezi, E., Kostenidou, E., Hildebrandt, L., Psichoudaki, M., Engelhart, G. J., et al. (2015). *Volatility of organic aerosol and its components in the Megacity of Paris*. https://doi.org/10.5194/acpd-15-22263-2015

Petters, M. D., & Kreidenweis, S. M. (2007). A single parameter representation of hygroscopic growth and cloud condensation nucleus activity. *Atmospheric Chemistry and Physics*, *7*(8), 1961–1971. https://doi.org/10.5194/acp-7-1961-2007

Rivellini, L.-H., Chiapello, I., Tison, E., Fourmentin, M., Féron, A., Diallo, A., et al. (2017). Chemical characterization and source apportionment of submicron aerosols measured in Senegal during the 2015 SHADOW campaign. *Atmospheric Chemistry and Physics*, *17*(17), 10291–10314. https://doi.org/10.5194/acp-17-10291-2017

Shah, R. U., Robinson, E. S., Gu, P., Robinson, A. L., Apte, J. S., & Presto, A. A. (2018). High-spatial-resolution mapping and source apportionment of aerosol composition in Oakland, California, using mobile aerosol mass spectrometry. *Atmospheric Chemistry and Physics*, *18*(22), 16325–16344. https://doi.org/10.5194/acp-18-16325-2018

Struckmeier, C., Drewnick, F., Fachinger, F., Gobbi, G. P., & Borrmann, S. (2016). Atmospheric aerosols in Rome, Italy: Sources, dynamics and spatial variations during two seasons. *Atmospheric Chemistry and Physics*, *16*(23), 15277–15299. https://doi.org/10.5194/acp-16-15277-2016

Thamban, N. M., Tripathi, S. N., Moosakutty, S. P., Kuntamukkala, P., & Kanawade, V. P. (2017). Internally mixed black carbon in the Indo-Gangetic Plain and its effect on absorption enhancement. *Atmospheric Research*, *197*, 211–223. https://doi.org/10.1016/j.atmosres.2017.07.007

Xiao, R., Takegawa, N., Zheng, M., Kondo, Y., Miyazaki, Y., Miyakawa, T., et al. (2011). Characterization and source apportionment of submicron aerosol with aerosol mass spectrometer during the PRIDE-PRD 2006 campaign. *Atmospheric Chemistry and Physics Discussions*, *11*. https://doi.org/10.5194/acp-11-6911-2011

Xu, J. Z., Shi, J., Zhang, Q., Ge, X., Canonaco, F., Prévôt, A. S. H., et al. (2016). Wintertime organic and inorganic aerosols in Lanzhou, China: Sources, processes, and comparison with the results during summer. *Atmospheric Chemistry and Physics*, *16*(23), 14937–14957. https://doi.org/10.5194/acp-16-14937-2016

Xu, L., Suresh, S., Guo, H., Weber, R. J., & Ng, N. L. (2015). Aerosol characterization over the southeastern United States using high-resolution aerosol mass spectrometry: Spatial and seasonal variation of aerosol composition and sources with a focus on organic nitrates. *Atmospheric Chemistry and Physics*, *15*(13), 7307–7336. https://doi.org/10.5194/acp-15-7307-2015

Young, D. E., Allan, J. D., Williams, P. I., Green, D. C., Flynn, M. J., Harrison, R. M., et al. (2015). Investigating the annual behaviour of submicron secondary inorganic and organic aerosols in London. *Atmospheric Chemistry and Physics*, *15*(11), 6351–6366. https://doi.org/10.5194/acp-15-6351-2015

Young, D. E., Kim, H., Parworth, C., Zhou, S., Zhang, X., Cappa, C. D., et al. (2016). Influences of emission sources and meteorology on aerosol chemistry in a polluted urban environment: Results from DISCOVER-AQ California. *Atmospheric Chemistry and Physics*, *16*(8), 5427–5451. https://doi.org/10.5194/acp-16-5427-2016

Yuan, B., Hu, W. W., Shao, M., Wang, M., Chen, W. T., Lu, S. H., et al. (2013). VOC emissions, evolutions and contributions to SOA formation at a receptor site in eastern China. *Atmospheric Chemistry and Physics*, *13*(17), 8815–8832. https://doi.org/10.5194/acp-13-8815-2013

Zhang, Y., Du, W., Wang, Y., Wang, Q., Wang, H., Zheng, H., et al. (2018). Aerosol chemistry and particle growth events at an urban downwind site in North China Plain. *Atmospheric Chemistry and Physics*, *18*(19), 14637–14651. https://doi.org/10.5194/acp-18-14637-2018

Zhao, J., Qiu, Y., Zhou, W., Xu, W., Wang, J., Zhang, Y., et al. (2019). Organic aerosol processing during winter severe haze episodes in Beijing. *Journal of Geophysical Research: Atmospheres*, *124*(17–18), 10248–10263. https://doi.org/10.1029/2019jd030832

Zhu, Q., Huang, X.-F., Cao, L.-M., Wei, L.-T., Zhang, B., He, L.-Y., et al. (2018). Improved source apportionment of organic aerosols in complex urban air pollution using the multilinear engine (ME-2). *Atmospheric Measurement Techniques*, *11*(2), 1049–1060. https://doi.org/10.5194/amt-11-1049-2018